

26 the ASMA tracers are noticed in 2015 compared to the long-term mean. A 30% (20%) decrease in
27 carbon monoxide (water vapor) at 100 hPa is observed in July over most of the ASMA region,
28 whereas in August the drop is strongly concentrated in the edges of the ASMA. Prominent increase
29 of O₃ (>40%) at 100 hPa is clearly evident within the ASMA in July, whereas in August the
30 increase is strongly located (even at 121 hPa) over the western edges of the ASMA. Further, the
31 temperature around the tropopause shows significant positive anomalies (~5K) within the ASMA
32 in 2015. The present results clearly reveal the El Niño induced dynamical changes caused
33 significant changes in the trace gases within the ASMA in summer 2015. Overall, warming of the
34 tropopause region due to the increased O₃ weakens the anticyclone and further supported the
35 weaker ASMA in 2015 reported by previous studies.

36 **Keywords:** Trace gases, El Niño, Asian summer monsoon anticyclone, tropopause

37 1. Introduction

38 The Asian summer monsoon anticyclone (ASMA) is a distinct circulation system in the upper
39 troposphere and lower stratosphere (UTLS) during northern hemisphere boreal summer, ~~and~~
40 centered at ~25°N and ~~extends-extending~~ roughly between 15°N to 40°N (Park et al., 2004; Randel
41 et al., 2010). It is encircled by the subtropical westerly jet stream to the north and by the equatorial
42 easterly jet to the south (Randel and Park, 2006). It is well recognized that the ASMA circulation
43 is a prominent transport pathway for troposphere pollutants to enter the stratosphere (Randel et al.,
44 2010). Previous studies have concluded that deep convection during summer monsoon can
45 effectively transport the pollutants, aerosols and tropospheric tracers from the boundary layer into
46 the UTLS region (Vogel et al., ~~2015~~2016; Santee et al., 2017). These transported pollutants, tracers
47 and aerosols become confined in the ASMA and, consequently, affect the trace gas composition in
48 the UTLS region (Randerl et al., 2010; Solomon et al., 2010; Riese et al., 2012; Hossaini et al.,

49 2015). It is clearly evident from the previous studies that the ASMA has a higher concentrations
50 of tropospheric tracers such as carbon monoxide (CO), hydrogen cyanide (HCN) and Methane
51 (CH₄) and lower concentrations of stratospheric tracers including Ozone (O₃) and nitric acid
52 (HNO₃) (Park et al., 2004; Li et al., 2005; Park et al., 2008; Randel et al., 2010; Vernier et al.,
53 2015; Yan and Bian, 2015; Yu et al., 2017; Santee et al., 2017; [Vernier et al., 2018](#)). The
54 comprehensive study on the climatological composition ~~within~~ the ASMA can be found in
55 Santee et al. (2017). The ASM convection and orographic lifting are the primary mechanisms for
56 the higher concentrations of the tropospheric tracers in the ASMA (Li et al., 2005; Park et al.,
57 ~~2007~~[2009](#); Santee et al., 2017). Apart from these trace gases a strong persistent tropopause-level
58 aerosol layer called as ‘Asian Tropopause Aerosol Layer’ (ATAL) also existed between 12 to 18
59 km within the ASMA and it was first detected from the CALIPSO measurements (Vernier et al.,
60 2011).

61 Similarly, higher concentrations of water vapor (WV) within the ASMA during the summer
62 monsoon is well documented in the literature (Gettelman et al., 2004; Park et al., 2007; Randel et
63 al., 2010; Bian et al., 2012; Xu et al., 2014; Jiang et al., 2015; Das and Suneeth, 2020). ~~It is~~ ~~W~~well
64 known that ~~the~~ most of the ~~water vapor~~WV enters the stratosphere through the tropical tropopause
65 ~~layer~~(Fueglistaler et al., 2009) and the temperature ~~presented~~ at the tropical tropopause ~~strongly~~
66 controls the WV entering the lower stratosphere (LS). It is ~~also~~ well documented that several
67 processes such as convection, strength of the Brewer-Dobson circulation, El Niño–Southern
68 Oscillation (ENSO) and Quasi-Biennial Oscillation (QBO) are responsible for the WV transport
69 to the UTLS region (Holton et al., 1995; ~~Jiang et al., 2010~~; Dessler et al., 2014; Jiang et al., 2015;
70 ~~Das and Suneeth, 2020~~). ~~Other factors such as gravity waves and horizontal advection can also~~
71 ~~influence the WV transport in the UTLS region. For example,~~ Khan and Jin (2016), studied the

72 effect of gravity waves on the tropopause and WV ~~in the over~~ Tibetan Plateau and reported that the
73 gravity wave is the source for the WV transport from the lower to higher altitudes. ~~The tropopause~~
74 ~~is higher within the ASMA during the summer monsoon period as compared the surrounding~~
75 ~~regions (Randel et al., 2010; Santee et al., 2017).~~ Recently, Das and Suneeth (2020) reported about
76 the distributions of WV in the UTLS over the ASMA during summer using 13 years of Aura
77 Microwave Limb Sounder observations. They concluded that WV in the UTLS region inside the
78 central part of ASMA is mostly controlled by horizontal advection and very less from the local
79 process and tropopause temperature in both summer and winter. ~~reported about the causative~~
80 ~~mechanism for the presence of high WV in the ASMA region. The authors concluded that the~~
81 ~~UTLS water vapor in the ASMA is mainly controlled by the advection and tropopause altitude.~~

82 Convection during the summer monsoon is one of the major sources to transport the boundary
83 layer pollutants into the UTLS region (Randel et al., 2010). It is well established fact that the ENSO
84 has a strong influence on convection and circulation changes over the Asian monsoon region
85 (Kumar et al., 1999; Wang et al., 2015; Gadgil and Francis, 2016). Enhanced (suppressed)
86 convection over the Asian monsoon region generally observed in the cold phase of ENSO (warm
87 phase of ENSO) known as La Niña (El Niño). Few studies have existed to date on the impact of
88 ENSO on the ASMA trace gas composition changes and its dynamical changes. For example, Yan
89 et al. (2018) reported the influence of ENSO on the ASMA with a major focus on how the ENSO
90 winter signal propagates into the following seasons. They showed the weaker O₃ transport into the
91 tropics during the onset of the ASMA after boreal winter El Niño events, but the difference between
92 El Niño and La Niña composites becomes insignificant in the summer. In another study, Tweedy
93 et al. (2018) demonstrated the impact of boreal summer ENSO events on O₃ composition within
94 the ASMA in different phases of ENSO events. They reported that the ASMA forms earlier and

95 stronger in the La Niña period that leads to greater equatorward transport of O₃-rich air from the
96 extra-tropics into the northern tropics than during El Niño periods. ~~Very +R~~Recently, Fadnavis et al.
97 (2019) reported higher concentrations of aerosol layers observed in the ATAL region during the El
98 Niño period over the northern part of South Asia. However, the above- mentioned studies are
99 mainly focused on changes in the ASMA with respect to ENSO on seasonal scales or mature stage
100 of monsoon (combined mean of July and August), ~~respectively~~.

101 Based on the above-mentioned studies, it ~~is can be~~ concluded that the ENSO also has a strong
102 influence on the ASMA structure and its composition. The recent 2015-16 El Niño event was
103 recorded as an extreme and long-lasting event in the 21st century (Huang et al., 2016; Avery et al.,
104 2017). ~~It was started as a weak El Niño during 2014-15 boreal winter and it developed as a strong~~
105 ~~boreal summer El Niño event in 2015 (Tweedy et al., 2018). Further, this strong boreal summer~~
106 ~~event was continued and significantly enhanced until the boreal winter of 2015-16. It was also one~~
107 ~~of the strongest El Niño events that occurred in the boreal summer (Tweedy et al., 2018).~~ In this
108 event, several unusual changes occurred in the tropical UTLS region including, the strong
109 enhancement in the lower stratosphere WV (higher positive tropopause temperature anomalies)
110 over ~~the~~ Southeast Asia and western Pacific regions (Avery et al., 2017) and anomalous distribution
111 of trace gases in the UTLS region (Diallo et al., 2018; Ravindra Babu et al., 2019a). Similar way,
112 the response of different trace gases (O₃, HCl, WV) to the disrupted 2015–2016 quasi-biennial
113 oscillation (QBO) associated with 2015-16 El Niño event is also reported by Tweedy et al. (2017).
114 Dunkerton (2016), discussed the possible role of unusual warm ENSO event in 2015-2016 to the
115 QBO disruption by triggering the extratropical planetary waves. Therefore, in the present study,
116 we ~~tried to investigate~~ the detailed changes observed in the ASMA 2015 particularly ~~by focused~~
117 ~~focusing~~ on the structure, dynamics and trace gases variability within the ASMA in July and

Formatted: Subscript

118 August 2015 by using satellite ~~measurements-observations~~ and reanalysis products. The present
119 research article is organized as follows. A ~~d~~Database and methodology adopted in this study are
120 discussed in Section 2. The results and discussions are illustrated in Section 3. Finally, the
121 summary and conclusions obtained from the present study are summarized in Section 4.

122 **2. Database and Methodology**

123 **2.1. Microwave Limb Sounder (MLS) measurements**

124 In the present study, version 4.2 Aura MLS measurements of CO, O₃ and WV are utilized.
125 The MLS data of July and August months in each year from 2005 to 2015 period are considered.
126 The vertical resolution for CO is in the range 3.5–5 km from the upper troposphere to the lower
127 mesosphere and the useful range is 215–0.0046 hPa. The horizontal resolution for CO is about 460
128 km at 100 hPa and 690 km at 215 hPa. For WV, the vertical resolution is in the range of 2.0 to 3.7
129 km from 316 to 0.22 hPa and the along-track horizontal resolution varies from 210 to 360 km for
130 pressure greater than 4.6 hPa. For O₃, the vertical resolution is ~2.5 km and the along-track
131 horizontal resolution varies between 300 and 450 km. The precision (systematic uncertainty) for
132 WV is ~ 10-40% (~10-25%), for O₃ is ~0.02–0.04 (~0.02–0.05) ppmv and for CO, it is ~ 19 ppbv
133 (30%), respectively. More details about the MLS version 4 level 2 data can be found in Livesey et
134 al. (2018).

135 **2.2. COSMIC Radio Occultation measurements**

136 To see the changes in the tropopause temperature and height within the ASMA, we used high-
137 resolution, post-processed products of level 2 dry temperature profiles obtained from Constellation
138 Observing System for Meteorology, Ionosphere, and Climate (COSMIC) Radio Occultation (RO).
139 Each month of July and August from 2006 to 2015 are considered. The data is downloaded from
140 the COSMIC Data Analysis and Archival Center (CDAAC) website. We used 200 m vertical

141 resolution temperature profiles in the study. Details of the temperature retrieval from the bending
142 angle and refractivity profiles obtained from the RO sounding are presented well in the literature
143 (Kursinski et al. 1997; Anthes et al. 2008). The COSMIC temperature have a precision of 0.1%
144 between 8 and 25 km (Kishore et al. 2009; Kim and Son, 2012). The temperature accuracy in the
145 UTLS is better than 0.5 K for individual profiles and ~0.1 K for averaged profiles (Hajj et al.
146 2004). It is noted that for individual RO temperature profiles, the observational uncertainty
147 estimate is 0.7 K in the tropopause region, slightly decreasing into the troposphere and gradually
148 increasing into the stratosphere (Scherllin-Pirscher et al., 2011a). For monthly zonal-averaged
149 temperature fields, the total uncertainty estimate is smaller than 0.15 K in the UTLS (Scherllin-
150 Pirscher et al., 2011b). Overall, the uncertainties of RO climatological fields are small compared
151 to any other UTLS observing system for thermodynamic atmospheric variables. Note that these
152 data are compared with a variety of techniques including GPS radiosonde data and observed good
153 correlation particularly in the UTLS region (Rao et al. 2009; Kishore et al. 2009). The COSMIC
154 RO profiles have been widely used for studying the tropopause changes and its variabilities (Kim
155 and Son, 2012; RavindraBabu et al. 2015; [RavindraBabu and Liou, 2021](#)).~~RavindraBabu et al.~~
156 ~~2019b~~).

157 **2.3. National Centers for Environmental Prediction (NCEP) Reanalysis data**

158 We also utilized monthly mean Geopotential height (GPH) and wind vectors (zonal and
159 meridional wind speed) from the [NCEP-DOE Reanalysis 2 \(Kanamitsu et al., 2002\)](#),~~National~~
160 ~~Centers for Environmental Prediction/National Center for Atmospheric Research (NCEP/NCAR)~~
161 ~~reanalysis (Kalnay et al., 1996)~~, covering the same time period as the MLS observations (2005-
162 2015). [NCEP-DOE Reanalysis 2 is an improved version of the NCEP Reanalysis I model that](#)
163 [fixed errors and updated parametrizations of physical processes.](#) The horizontal resolution of

164 ~~NCEP/NCAR~~ NCEP-DOE Reanalysis 2 is $2.5^\circ \times 2.5^\circ$, respectively.

165 Apart from the above-mentioned data sets, we also used European Centre for Medium-Range
166 Weather Forecasts (ECMWF) interim reanalysis potential vorticity (PV) data particularly at 350K
167 isentropic surface in July and August 2015 (ERA-Interim; Uppala et al., 2005; Dee et al., 2011).

168 **2.5. Methodology**

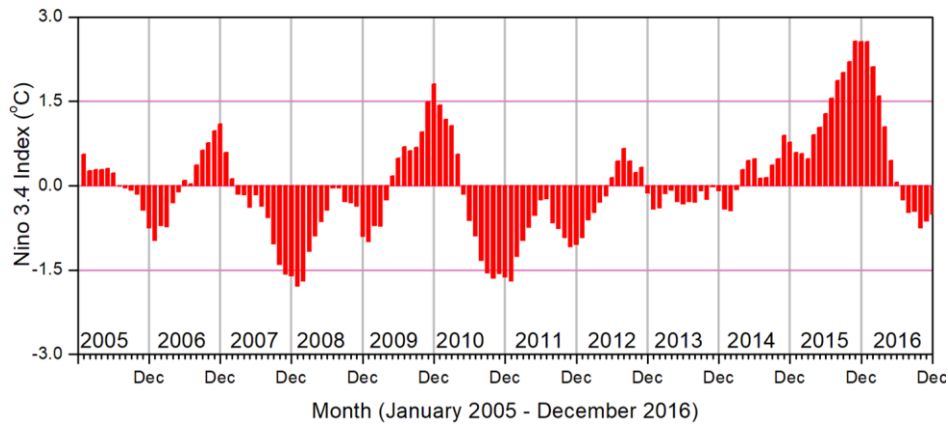
169 Daily available MLS profiles of O₃, CO, and WV in each month are constructed and gridded
170 by averaging the profiles inside bins with a resolution of 5° latitude \times 5° longitudes. The following
171 equation is used to estimate the relative change in percentage.

$$172 \quad \text{Relative change in percentage} = \left(\frac{x_i - \bar{x}}{\bar{x}} \right) \times 100 \quad (1)$$

173 where x_i represents the monthly mean of July/August in 2015, and \bar{x} is the corresponding monthly
174 long-term mean which is calculated by using the data from 2005 to 2014.

175 **3. Results and Discussion**

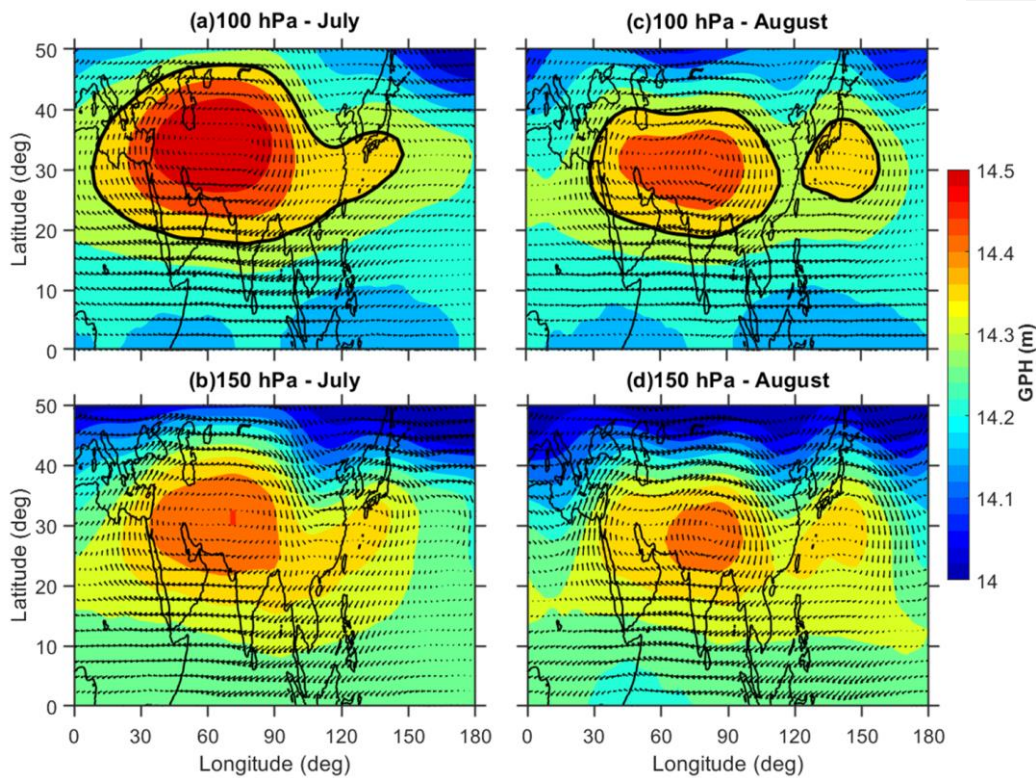
176 It is well reported that the ASMA is highly dynamic in nature with respect to its position and shape.
177 Also it varies at different time scales i.e day-to-day, weekly and monthly scales caused by internal
178 dynamical variability (Randel and Park, 2006; Garny and Randel, 2013; Pan et al., 2016; Nützel
179 et al., 2016; Santee et al., 2017). The intensity and spatial extension of the ASMA are prominent
180 in July and August where the monsoon was in the mature phase (Santee et al., 2017; Basha et al.,
181 2019). It can be noticed that the 2015-16 El Niño event was one of the strongest boreal summer
182 events that occurred in the entire MLS data record (Tweedy et al., 2018). In this event, the Nino
183 3.4 data was exceeded +1.5 in July and +1.8 in August (**Fig. 1**). Therefore, in the present study,
184 we mainly focused on ASMA behavior and trace gases changes ~~in~~ within the ASMA on monthly
185 scales particularly in July and August 2015 which represents strong El Niño.



186
 187 **Figure 1.** Temporal evolution of observed Niño3.4 Index data from January 2005 to December
 188 2016.

189 **3.1. Structure and dynamical changes in ASMA during 2015**

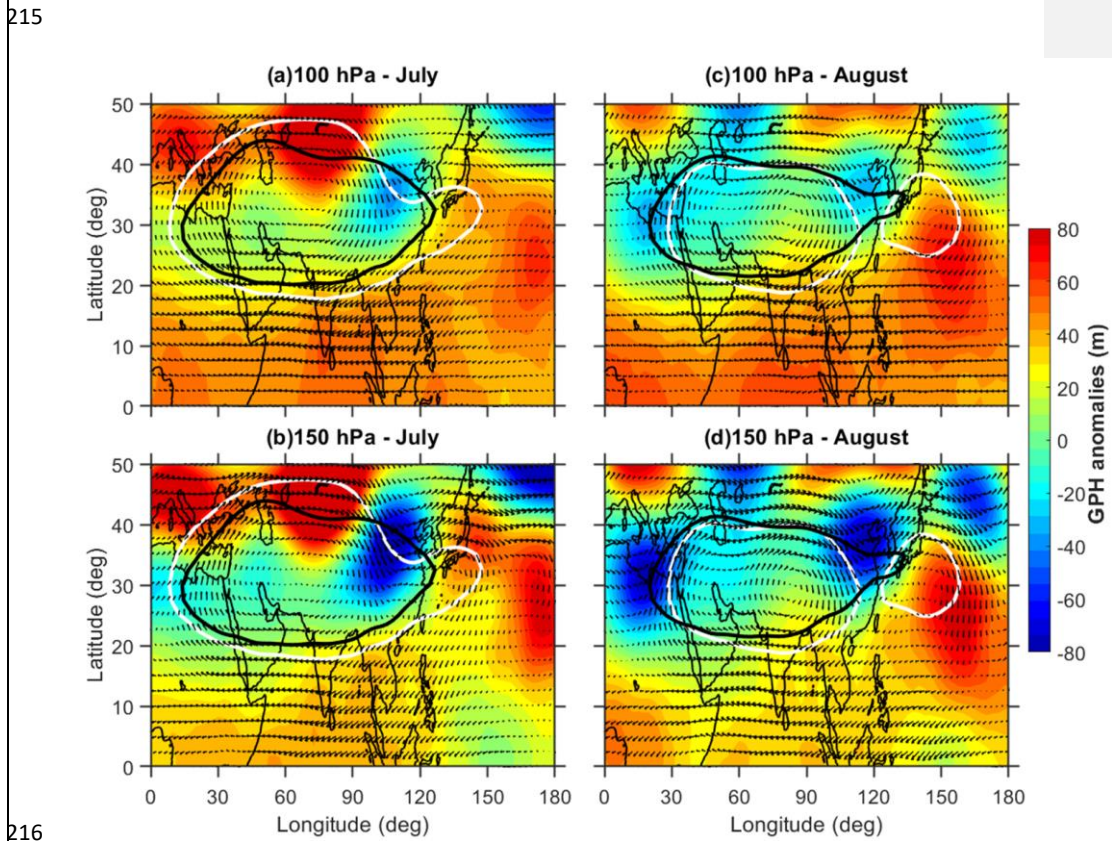
190 In general, the studies looking at monthly or seasonal timescales related to the thermo-
 191 dynamical features in the ASMA, the anticyclone region is mostly defined from the simple
 192 constant GPH contours at different pressure levels (Randel and Park, 2006; Yan et al., 2011;
 193 Bergman et al., 2013; Basha et al., 2019). Previous researchers used different GPH contours at 100
 194 hPa to define the anticyclone region. For example, Yan et al. (2011) used 16.7 km, Bergman et al.
 195 (2013) used 16.77 km and recently Basha et al. (2019) used 16.75 km GPH contour as the
 196 anticyclone region. In a similar manner, we also defined the ASMA region based on [NCEP-DOE](#)
 197 [Reanalysis 2 obtained NCEP reanalysis](#) GPH at 100 hPa and considered the 16.75 km GPH contour
 198 as the anticyclone region.



199
 200 **Figure 2.** Spatial distribution of geopotential height ~~observed~~ obtained from NCEP-DOE
 201 Reanalysis 2 data in during July 2015 (a) at 100 hPa and (b) 150 hPa superimposed with wind
 202 vectors at the respective corresponding levels. Subplots of (c) and (d) are the same as (a) and (b)
 203 but for the month of August. The black color solid contour lines represent the ASMA region at 100
 204 hPa (16.75 km GPH contour).

205 The spatial distribution of GPH at 100 hPa and 150 hPa for the month of July (August) is
 206 shown in **Fig. 2a and 2b (Fig. 2c and 2d)**. The corresponding monthly mean winds at respective
 207 pressure levels are also shown in **Fig.2**, respectively. The black solid line represents the ASMA
 208 region at 100 hPa based on 16.75 km GPH contour. The GPH distribution in **Fig. 2** shows clear
 209 distinct variability in the ASMA spatial structure between July and August at both pressure levels.

210 For example, at 100 hPa, the maximum GPH center was located over western side in July whereas
 211 it was located over near to the Tibetan region in August. Interestingly the ASMA itself separated
 212 into two anticyclones (16.75 km GPH contour black solid line in the figure) in August compare to
 213 July. The center of the small anticyclone was located over the ~~northwestern~~ Northwestern pacific
 214 Pacific near 140°E with the closed circulation indicated by the wind arrows.



217 **Figure 3.** Spatial distribution of geopotential height anomalies obtained from NCEP-DOE
 218 Reanalysis 2 data observed in during July 2015 (a) at 100 hPa and (b) 150 hPa superimposed with
 219 wind vectors at the respective corresponding levels. (c) and (d) same as (a) and (b) but for the
 220 month of August. The white color solid contour lines represent the ASMA region at 100 hPa (16.75

221 km GPH contour) observed in 2015 whereas the black color line represents the mean of 2005-
222 2014.

223 Further, we compared the ASMA structure in 2015 with referenced long-term mean. For
224 this, we obtained the GPH anomalies by subtracting the background long-term mean (2005-2014)
225 from 2015. **Fig-3Figure 3** shows the latitude-longitudinal distribution of GPH anomalies (color
226 shaded) along with wind vectors depicting circulation pattern at 100 hPa as well as at 150 hPa
227 during July and August. The white (black) color contour represents 16.75 km GPH at 100 hPa for
228 the corresponding month in 2015 (long-term mean). The GPH anomalies at both pressure levels
229 show quite different features in July and August. A clear wave-like structures can be observed
230 from the GPH anomalies. In July, the GPH anomalies exhibit strong negative maxima over 25-
231 40°N, 90-120°E and positive maxima over 40-50°N, 60-80°E regions. The 16.75 km GPH contour
232 lines in the ASMA region exhibits higher extension in all the directions except over the
233 northeastern edges of the ASMA in July compared to the long-term mean. At the same location
234 (northeastern edges), the ASMA exhibits a pronounced southward extension in July. Distinct
235 features of GPH anomalies are noticed in August as compared to July. In August, the strong
236 negative GPH anomalies are situated over the west and north-eastern edges of the ASMA.

237 It is well known that the subtropical westerly jet is an important characteristic feature of
238 the ASMA (Ramaswamy 1958), and thus its changes during 2015 are also investigated. As the
239 peak intensity of the westerly jet was located at 200 hPa (Chiang et al., 2015), we focused mainly
240 on 200 hPa zonal wind changes in July and August. **Fig-Figure 4a and 4c (Fig. 4b and 4d)** show
241 the spatial distribution of long-term (2015) monthly mean zonal wind at 200 hPa during July and
242 August. In general, the subtropical westerlies are located near to ~40°N latitude during the mature
243 phase of the monsoon period (Chiang et al., 2015). Compared to long-term mean, a significant
244 weakening of the subtropical westerlies is noticed in 2015. Further, a strong southward shift in the

245 westerlies is observed over the northeastern Asia region. This southward shift is moved even up
246 to 30°N in both months. From zonal wind at 200 hPa (**Fig. 4**) and wind vectors at 100/150 hPa
247 (**Fig. 2**), it is clear that anomalous changes have occurred in the subtropical westerlies over the
248 northeastern parts of the AMSA around 30-40°N, 90-120°E during July and August 2015. The
249 southward shift in the westerlies is strongly associated with the southward extension of the ASMA
250 over the northeastern side of the ASMA (**Fig. 2**). This is strongly supported by the previous
251 findings by Lin and Lu (2005) where they showed the southward extension of the South Asian
252 High could lead to the southward shift of the ~~westerly~~westerlies.

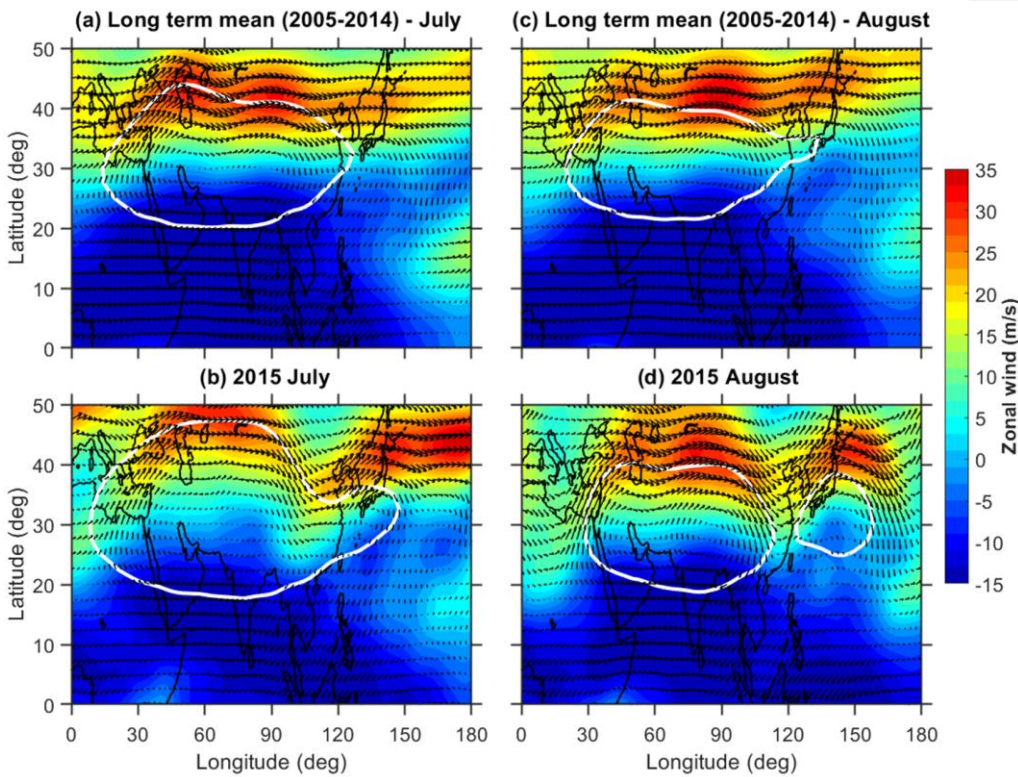


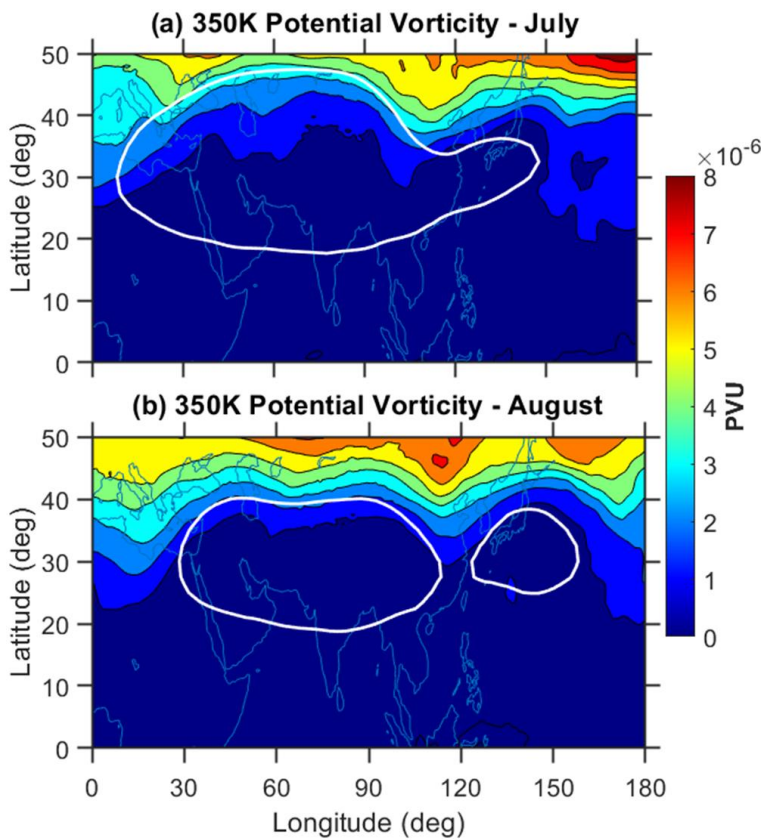
Figure 4. Spatial distribution of monthly mean zonal winds ~~observed~~obtained from NCEP-DOE

256 Reanalysis 2 data at 200 hPa ~~in~~-during July during (a) 2005-2014 (b) 2015 year. (c) and (d) same
257 as (a) and (b) but for the month of August. The white color solid contour lines represent the ASMA
258 region at 100 hPa (16.75 km GPH contour).

259 From the GPH and winds observations, it is clear that pronounced changes are evident in
260 the dynamical structure of the ASMA in 2015 and also relatively different features are noticed
261 between July and August months. Interestingly the ASMA itself separated into two anticyclones
262 during August 2015 and the separation exactly coincided with the strong negative GPH anomalies
263 and southward meandering of subtropical westerlies over the northeastern side of the ASMA. The
264 ~~western-Western pacific-Pacific (WP)~~ mode of the anticyclone is visible in August. The split of
265 the anticyclone and the formation of the ~~western-Pacific (WP)~~ mode are in agreement with previous
266 studies reported by few researchers earlier (e.g. Homomichl and Pan, 2020). The presence of the
267 WP mode may be due to the eastward eddy shedding of the ASMA system in the process of its
268 sub-seasonal zonal oscillation (Homomichl and Pan, 2020) or Rossby wave breaking (RWB) in the
269 subtropical westerly jet (Fadnavis and Chattopadhyay, 2017). Fadnavis and Chattopadhyay (2017)
270 also identified the split of ASMA into two anticyclones: one over Iran and another over the Tibetan
271 region due to the RWB in June 2014 monsoon period. To see any signatures of these RWB in 2015,
272 we further analyzed the RWB through the ERA interim reanalysis potential vorticity (PV) data.
273 Based on previous studies, it is reported that RWBs can be identified from PV distribution at 350
274 K isentropic surface (Samanta et al. 2016; Fadnavis and Chattopadhyay, 2017). We used 350_K
275 isentropic surface PV data in July and August 2015 in the present analysis.

276 **Figure 5a–b** shows the distribution of ERA interim monthly mean PV at the 350 K
277 isentropic surface during July and August 2015. It can be seen that, during July and August 2015,
278 clear RWB signatures evident near 100°E. It is noted that the equatorial advection of high PV
279 values with a steep gradient and the southward movement of PV from the westerly jet are the basic

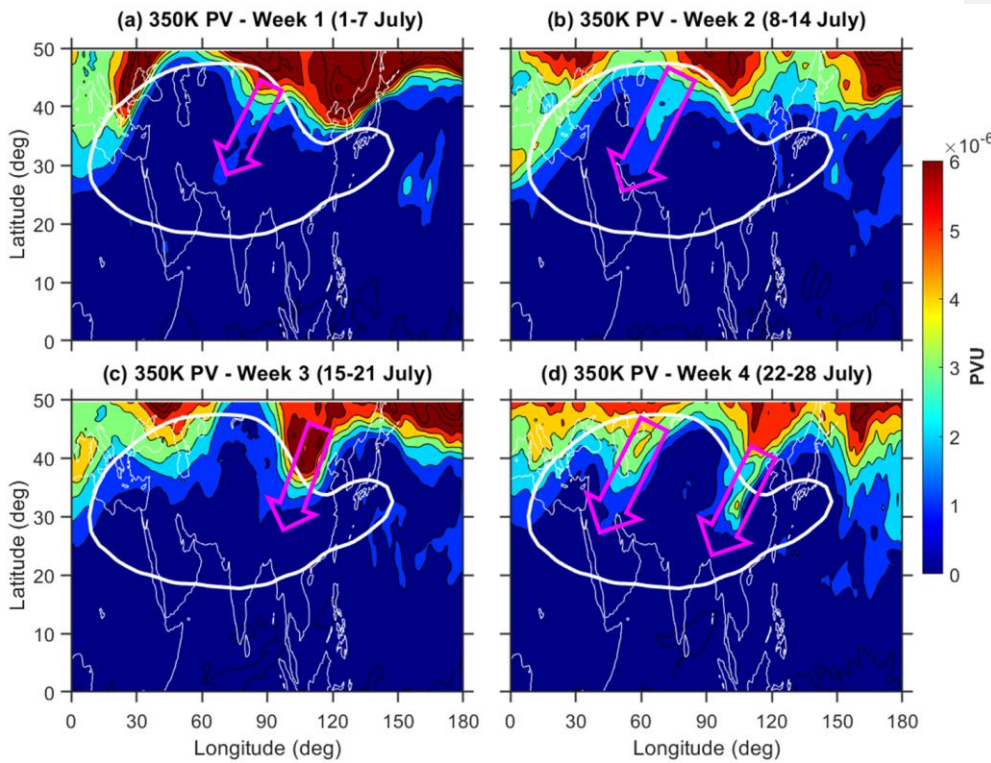
280 features of the RBW (Vellore et al., 2016; Samanta et al. 2016). These features are clearly exhibited
281 in **Figure 5** with higher PV values extends up to $\sim 30^\circ\text{N}$ in both months over 100°E region. The
282 location of this RBW is significantly correlated with a southward meandering of westerlies and
283 strong negative GPH anomalies. However, the observed RBW signatures in both months are from
284 monthly mean PV data. Further, to see the clear signatures of these RBW, we made weekly based
285 analysis for July month. For this we considered 1-7 July as week-1 and 8-14 July as week-2 so on.
286 The weekly mean distribution of 350K isentropic surface PV during July is shown in **Figure-Fig.**
287 **6.**



288

289 **Figure 5.** ERA Interim observed spatial distribution of potential vorticity (PV) on a 355-350 K
290 isentropic surface in PVU ($1 \text{ PVU} = 10^{-6} \text{ K m}^2 \text{ kg}^{-1} \text{ s}^{-1}$) ($10^{-6} \text{ kg m}^2 \text{ s}^{-2} \text{ K}$): (a) monthly mean of
291 July and (b) monthly mean of August 2015. The white color solid contour lines represent the
292 ASMA region at 100 hPa (16.75 km GPH contour). Red color contours represent the anticyclone
293 region during the respective months. The outer contour represents 16.75 km and the inner contour
294 for 16.85 km geopotential height. Black arrows indicate the regions of RWB.
295 The black-magenta colored arrows which are shown in the figure-Fig. 6 represents the RWB events
296 during July 2015. A clear signature of air with high values of PV traverses from extra-tropics to
297 ASMA is evident from Fig.6. At weekly scales, clear RWB signatures are observed over the
298 anticyclone region. For example, in week-1 and week-2, the RWB signatures are evident over the
299 northern region of the ASMA. However, in week-3 and week-4, these RWB signatures are very
300 clear over northeastern Asia. Even-even in week-5 (29July-04August), we noticed RWB signatures
301 in PV data (Figure not shown). This clearly shows that The RWB splits the ASMA into two
302 anticyclones: one over the Tibetan region and another over the WP region. It is clear that the
303 equatorward penetration of extra tropical forcing through the subtropical westerly jet is has started
304 in July and further amplified by the splitting of the ASMA into two during August.

Formatted: Superscript



305
 306 **Figure 6.** Same as **Figure 5**, but for the weekly distribution of PV in July 2015. **Black-Magenta**
 307 **colored** arrows indicate the regions of RWB.

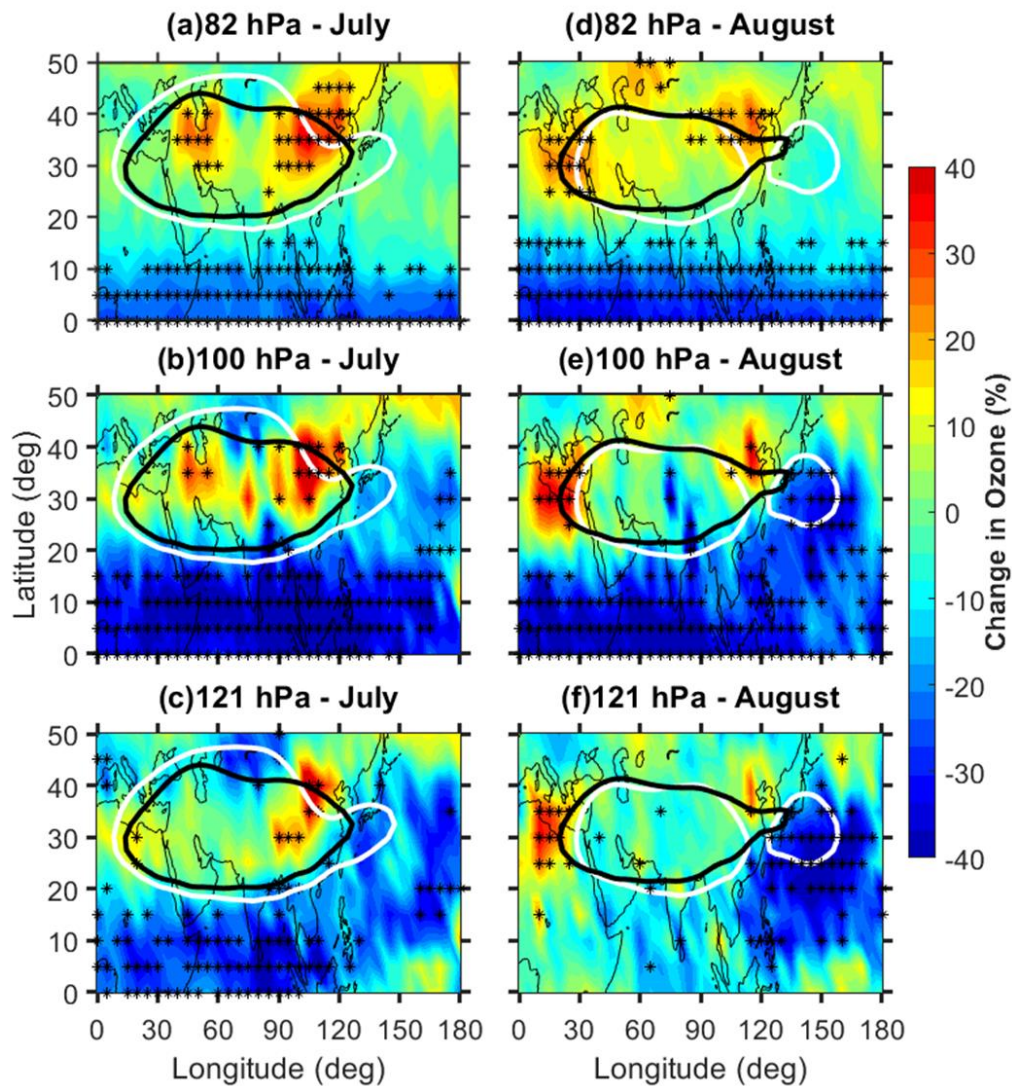
308 It is well known that the RWB is an important mechanism for horizontal transport between
 309 the extratropical lower stratosphere to the tropical UTLS region. These RWBs can act as an agent
 310 for the transport of extratropical stratospheric cold, dry, and O₃-rich air into the ASMA during the
 311 summer monsoon. Overall, it is concluded that the combination of the RWBs and strong southward
 312 meandering of the subtropical westerly jet in 2015 causes significant dynamical and structural
 313 changes in the ASMA. These changes in the ASMA dynamical structure in 2015 can influence the
 314 concentrations of the different trace gases within the ASMA. **Further, we quantified the changes**
 315 **in O₃, CO and WV concentrations within the ASMA during 2015 caused by the dynamical**

Formatted: Subscript

316 ~~effects. Further we studied how much percentage change occurred in the O₃ concentration and other~~
317 ~~tropospheric tracers with in the ASMA during 2015 due to these dynamical changes. For this we~~
318 ~~extensively utilized MLS satellite trace gases measurements.~~ The changes that occurred in the O₃
319 and CO, WV, are discussed in the following sections.

320 3.2. Trace gases anomalies observed within the ASMA in 2015

321 ~~It is well-documented that the ASMA contains low (high)~~ Well reported that the ASMA has
322 ~~low (high)~~ concentrations of stratospheric tracers such as O₃ (tropospheric tracers such as CO, WV
323 and etc.) and higher tropopause height compared to the region outside the ASMA during boreal
324 summer (Park et al., 2007; Randel et al., 2010; Santee et al., 2017; Basha et al., 2019). Differences
325 ~~of the trace gases within and outside of the ASMA are attributed to~~ Remarkable variabilities of
326 ~~these trace gases are attributed to~~ the strong winds and closed streamlines associated with the
327 ASMA, which act to isolate the air (Randel and Park 2006; Park et al. 2007). ~~As mentioned in the~~
328 ~~introduction, the monsoon in 2015 was strongly affected by the strong El Niño conditions in July~~
329 ~~and August 2015. Based on the previous studies, the summer monsoon in 2015 was reported as a~~
330 ~~weaker monsoon and the ASMA circulation also relatively weak (Yuan et al., 2018; Tweedy et al.,~~
331 ~~2018).~~ To see the changes in the trace gases during 2015, we generated the background long-term
332 mean of CO, O₃, and WV by using 10 years of MLS trace gas data from 2005 to 2014. Here the
333 results are discussed mainly based on the percentage changes relative to the respective long-term
334 monthly mean trace gases using Equation Equ. 1.



336
 337 **Figure 7.** Ozone relative percentage change in July 2015 with respect to background
 338 climatological monthly mean observed at (a) 82 hPa, (b) 100 hPa and (c) 121 hPa. (c) and (d) same
 339 as (a) and (b) but for the month of August. The white (black) color contour represents 16.75 km
 340 geopotential height at 100 hPa for the corresponding month in 2015 (mean of 2005-
 341 2014 climatological). The star symbols (black) shown in figure represent the anomalies greater than

342 the $\pm 2\sigma$ standard deviation of long-term mean. The results are obtained from MLS measurements.

343 **Fig-Figure 7a-c (Fig. 7d-f)** shows the distribution of relative percentage change in the O₃
344 concentrations within the anticyclone ASMA at 82 hPa, 100 hPa and 121 hPa during July (August)
345 2015. The anomalies larger than $\pm 2\sigma$ standard deviation of long-term mean are highlighted with
346 star symbols in the respective figures. The spatial distribution of changes in the O₃ (Fig. 7) shows
347 a clear increase in the O₃ mixing ratios (>40%) within the ASMA in 2015. The observed increase
348 within the ASMA is quite distinct between July and August. In July, the O₃ shows a pronounced
349 increase within the ASMA at all the pressure levels. Note that the observed increase was
350 statistically significant with larger than 2σ standard deviation of long-term mean (see the star
351 symbols). This increase is quite significant over the northeastern edges of the ASMA and quite
352 high at 100 hPa compared to 82 hPa and 121 hPa. In August, the O₃ shows quite different features
353 compared to July (Fig. 7d-f). A strong increase in the O₃ is observed over the western and eastern
354 edges of the ASMA at all the pressure levels. The increase is quite significant at 100 hPa and even
355 at 121 hPa. The increase of O₃ is still appearing over the northeastern edges of the ASMA in August
356 as observed in July. Overall, a significant enhancement of O₃ within the ASMA is clear evidence
357 in July and August 2015.

358 The significant increase of O₃ within the ASMA in 2015 might be due to the transport from
359 the mid-latitudes through the STJ and also due to the stratosphere to the troposphere transport. For
360 example, the strong enhancement of O₃ within the ASMA at 100 hPa in July was strongly matched
361 with the observed high values of PV at 350 K isentropic surface (Fig. 6). This is further supported
362 by the strong southward meandering of STJ in July (Fig. 3), respectively. Thus, a clear transport
363 of mid-latitude air with high PV and high O₃ is evident during 2015. At the same time, the
364 enhancement of O₃ was clearly observed at all the pressure levels from 82 hPa to 121 hPa which
365 is further supported for the stratosphere to the troposphere transport. Note that 82 hPa can represent

Formatted: Subscript

Formatted: Subscript

Formatted: Subscript

Formatted: Subscript

Formatted: Subscript

Formatted: Subscript

Formatted: Subscript

366 the lower stratosphere and 121 hPa for the upper troposphere (Das et al., 2020). It can be noticed
367 that the ASMA is strongly associated with troposphere-stratosphere transport as well as
368 stratosphere-troposphere transport (Garny and Randel, 2016; Fan et al., 2017). Also, it is well
369 reported that the northern part of the ASMA is an active region for stratosphere-troposphere
370 transport processes (Sprenger et al., 2003; Škerlak et al., 2014).

371 Similarly, significant lowering of O₃, particularly at 100 hPa and 82 hPa is clearly noticed
372 over the tropics (Fig. 7). This is quite expected due to the enhanced tropical upwelling (bringing
373 poor O₃ air from troposphere) caused by the strong El Niño conditions in July and August 2015.

374 As mentioned in the previous sections, strong El Niño conditions are clearly evident in July and
375 August 2015 (Fig. 1). The observed strong negative O₃ anomalies over the tropics from the present
376 study are well matched with the previous studies (Randel et al., 2009; Diallo et al., 2018). From
377 the present results, it is very clear that there is a significant decrease over the tropics and the
378 increase over the mid-latitudes in 2015. These changes observed in the O₃ (decrease and increase)

379 are attributed due to the strengthening of the tropical upwelling and enhanced downwelling from the
380 shallow branch of the Brewer-Dobson circulation in the mid-latitudes due to the strong El Niño
381 conditions in 2015. Overall, it is concluded that initially, during July, the O₃ is transported into the
382 anticyclone from the northeastern edges of the ASMA region through the sub-tropical westerlies
383 and then it is isolated within the ASMA region. This is further supported by the southward
384 meandering of the westerly jet and southward shift of the ASMA (negative GPH anomalies) over
385 the same region in July (Fig. 3). Also, significant transport of mid-latitude dry air is clear from the
386 Fig. 6. Thus, it is clear from the results that the stratosphere to troposphere transport and horizontal
387 advection along with the subtropical jet caused the strong enhancement of the O₃ within the ASMA
388 in 2015.

Formatted: Subscript

Formatted: Subscript

Formatted: Subscript

389 Distinct features are evident in the O_3 changes between July and August. Also, the observed
390 changes in the O_3 are well correlated with the observed GPH anomalies in both months (Fig. 3).
391 In July, the O_3 shows a pronounced increase in the ASMA at all the pressure levels. This increase
392 is quite significant over the northeastern edges of the ASMA and quite high at 100 hPa compared
393 to 82 hPa and 121 hPa. A more than 40% increase is found at 100 hPa particularly over the
394 northeastern edges of the ASMA in July. Even at 82 hPa and 121 hPa, significant enhancement in
395 the O_3 concentrations are evident over the northeastern edges of the ASMA during July. This
396 enhancement is clearly matching with the O_3 transport from higher latitudes which is shown in
397 Fig. 6 on a weekly scale from ERA interim data. Overall in July, the O_3 shows a prominent increase
398 over the northeastern edges of the ASMA at all the mentioned pressure levels and strongly
399 supported the stratosphere-troposphere transport over the same region. It can be noticed that the
400 ASMA is strongly associated with troposphere-stratosphere transport as well as stratosphere-
401 troposphere transport (Gamy and Randel, 2016; Fan et al., 2017). Also it is well reported that the
402 northern parts of the ASMA is an active region for stratosphere-troposphere transport processes
403 (Sprenger et al., 2003; Škerlak et al., 2014).

404 In August, the O_3 shows quite different features compared to July. A strong increase in the O_3
405 is observed over the western and eastern edges of the ASMA at all the pressure levels. The increase
406 is quite significant at 100 hPa and even at 121 hPa. And the observed increase is found 40%
407 compared to the long term mean at respective pressure levels. Even over the northeastern edges of
408 the ASMA, the increase of O_3 still appeared in August as observed in July. It is noted that in July
409 and August 2015, strong El Niño conditions have existed. We can expect a strong downwelling of
410 the shallow branch of Brewer-Dobson circulation in the mid-latitudes (Diallo et al., 2018).
411 Enhanced tropical upwelling over the tropics and strengthening of the downwelling in the northern

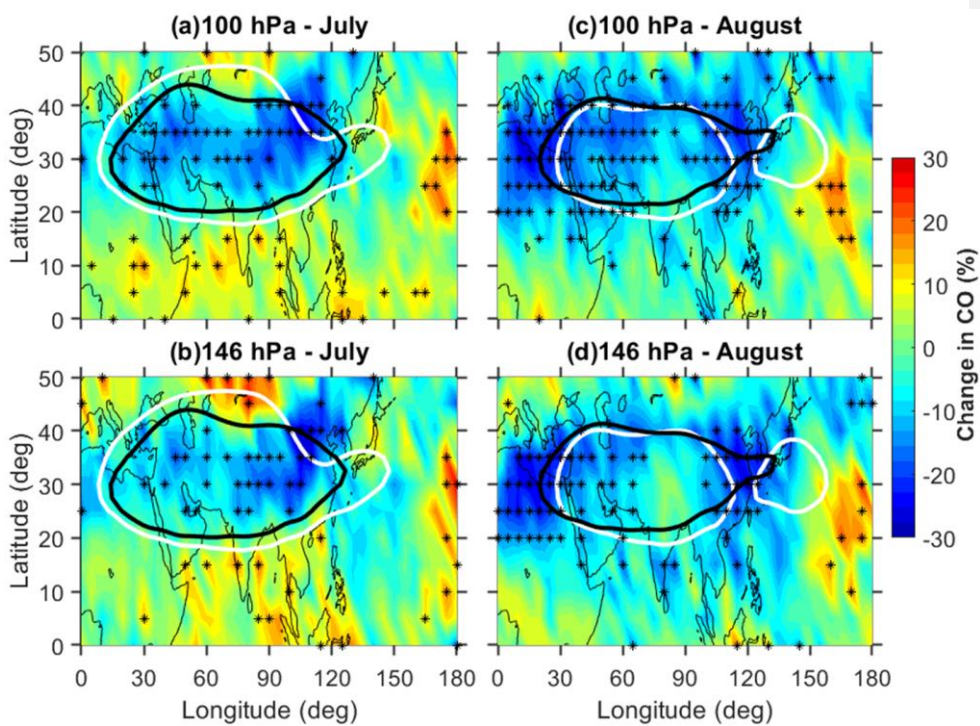
Formatted: Subscript

412 hemisphere mid-latitudes are likely to cause for the observed higher O₃ in the northern mid-
413 latitudes during El Niño. Due to the enhanced tropical upwelling, stronger ozone transport from
414 the tropics to the mid-latitudes is expected (Diallo et al., 2018). This clearly explains the observed
415 high O₃ in the ASMA during 2015. Initially, during July, the O₃ is transported into the anticyclone
416 from the northeastern edges of the ASMA region through the sub-tropical westerlies and then it is
417 isolated within the ASMA region. This is further supported by the southward meandering of the
418 westerly jet and southward shift of the ASMA (negative GPH anomalies) over the same region in
419 July (Fig. 3). Also from the Fig. 6, very clear transport of mid-latitude dry air into the ASMA
420 through the intrusions is seen. Thus, it is clear from the results that the stratosphere to troposphere
421 transport of O₃ along with the subtropical jet caused the strong enhancement of the O₃ within the
422 ASMA in July 2015. The confined O₃ within the anticyclone during July further separated from
423 the anticyclone and transported to the tropics as well as to the extra-tropics over the western edges
424 of the ASMA (~30°N) in August 2015.

425 **Fig-Figure 8a-b (Fig. 8c-d)** shows the spatial distribution of CO relative percentage change
426 at 100 hPa and 146 hPa observed in during July (August) 2015. The white (black) color contour
427 represents 16.75 km GPH at 100 hPa for the corresponding month in 2015 (climatological mean).
428 The observed changes in the CO clearly exhibit quite distinct features between July and August as
429 observed in the O₃. A significant decrease (~30%) is noticed in the CO concentrations over most
430 of the AMSA in July. The maximum decrease of CO is noticed over the northeastern edges of the
431 ASMA, located ~ 30-45°N, 90-120°E region. Whereas in August, the decrease of CO is more
432 concentrated over the east and western edges of the ASMA at both the pressure levels. Overall, the
433 MLS observed CO was ~30% below average (percentage decrease) compared to the climatological
434 monthly mean within the ASMA in July and edges of the ASMA in August 2015. It is noted that

Formatted: Subscript

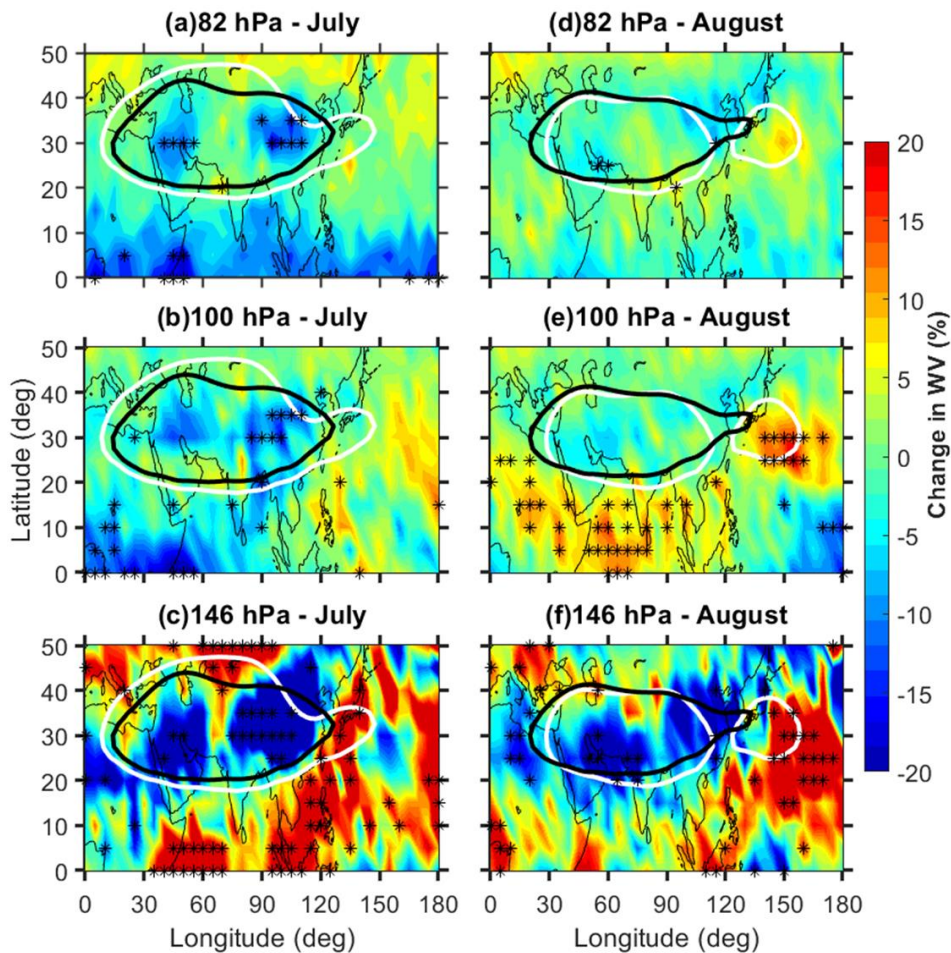
435 there is a considerable year-to-year variability of the CO sources over the ASM region (Santee et
 436 al., 2017). The major sources of the CO over the ASM region are from the biomass burning and
 437 industrial emission. The observed decreased CO within the ASMA in 2015 might be due to the
 438 year-to-year variability in the CO sources and the weaker vertical transport due to the El Niño
 439 conditions in 2015.



440
 441 **Figure 8.** Carbon monoxide relative percentage change in-during July 2015 with respect to
 442 climatological monthly mean observed at (a) 100 hPa and (b) 146 hPa. (c) and (d) same as (a) and
 443 (b) but for the month of August. The white (black) color contour represents 16.75 km geopotential
 444 height at 100 hPa for the corresponding month in 2015 (mean of 2005-2014). The star symbols
 445 (black) shown in figure represent the anomalies greater than the $\pm 2\sigma$ standard deviation of long-
 446 term mean. The results are obtained from MLS measurements.

447 Similarly, the WV relative percentage change at 82 hPa, 100 hPa and 146 hPa in July (August)

448 2015 are shown in **Fig. 9a-b-c** (**Fig. 9e9d-df**). The WV shows quite different changes at ~~both-all~~
449 the pressure levels in July and August. At 146 hPa, the WV exhibits a strong decrease ($> 20\%$)
450 within the ASMA in July as well as in August also. However, at 100 hPa and 82 hPa, the WV
451 shows a relatively significant decrease within the ASMA in July compared to August. From the
452 WV observations, it is concluded that the WV is strongly decreased at 146 hPa in both months.
453 Whereas at 100 hPa and 82 hPa, the decrease in WV is quite high in July compared to August. It
454 is also observed from the Fig. 9 that there is a significant enhancement of WV over the tropics at
455 146 hPa in both months. But the WV enhancement is quite significant at 100 hPa, particularly
456 during August compared to July. This enhancement in the WV around the tropical tropopause
457 region in August is quite expected due to the El Niño conditions (Randel et al., 2009; Konopka et
458 al., 2016). Overall, the tropospheric tracers (CO and WV) significantly decreased ($\sim 30\%$ and 20%)
459 within the ASMA during July and August 2015. These changes in the tropospheric tracers are
460 might be due to the weaker vertical motions during the 2015 monsoon. A weaker vertical transport
461 from the boundary layer to the UTLS is generally observed over the ASM region during El Niño
462 period (Fadnavis et al., 2019). The El Niño conditions will suppress the monsoon convection and
463 cause weaker vertical transport during monsoon. Also it is Well reported that the summer monsoon
464 in 2015 was weaker monsoon due to the strongest El Niño conditions existed in 2015 (Tweedy et
465 al., 2018; Yuan et al., 2019; Fadnavis et al., 2019). ~~These El Niño conditions will suppress the~~
466 ~~monsoon convection and cause weaker vertical transport during monsoon.~~



467
 468 **Figure 9.** Water vapour relative percentage change in July 2015 with respect to background
 469 climatological monthly mean observed at (a) 82 hPa, (b) 100 hPa and (c) 146 hPa. (c) and (d) same
 470 as (a) and (b) but for the month of August. The white (black) color contour represents 16.75 km
 471 geopotential height at 100 hPa for the corresponding month in 2015 (mean of 2005-2014). The star
 472 symbols (black) shown in figure represent the anomalies greater than the $\pm 2\sigma$ standard deviation
 473 of long-term mean. The results are obtained from MLS measurements.

474 From these results, it is clear that the enhancement of O_3 and lowering of CO/WV is evident
 475 in July and August 2015 compared to the climatological long-term monthly mean. The observed

476 high O₃ and low WV within the ASMA from the present study are consistent and well-matched
477 with the previous study reported by Li et al. (2018). They demonstrated the importance of the
478 large-scale atmospheric dynamics and the stratospheric intrusions for high O₃ and low WV over
479 Lhasa within the ASMA by using in-situ balloon-borne measurements. The O₃/WV changes
480 strongly influence the background temperature structure within the UTLS region (Venkat Ratnam
481 et al., 2016; RavindraBabu et al., 2019b). Further, we ~~tried to~~ investigated the tropopause
482 temperature changes within the ASMA by using COSMIC RO data. The results are presented in
483 the next following section.

484 3.3. Tropopause temperature anomalies in 2015

485 It is well known that the tropopause plays a crucial role in the exchange of WV, O₃ and other
486 chemical species between the troposphere and the stratosphere. Most of these exchanges (WV to
487 the lower stratosphere and O₃ to the upper troposphere) known as stratosphere troposphere
488 exchange (STE) take place around the tropopause region (Fueglistaler et al., 2009; Venkat Ratnam
489 et al., 2016; Ravindra Babu et al., 2019b). It is well reported that the tropopause within the ASMA
490 is higher than the outside regions at the same latitude (Randel et al., 2010; Santee et al., 2017). It
491 is a well known feature that the tropopause is higher over the ASMA than the surrounding regions
492 (Randel et al., 2010; Santee et al., 2017). Also well documented that most of the STE processes
493 that include WV and O₃ transport between troposphere and stratosphere are occur through the
494 tropopause (Fueglistaler et al., 2009; Ratnam et al., 2016; Ravindra Babu et al., 2015, 2019b,
495 2020). In the present study, we mainly focused on changes in the cold point tropopause temperature
496 (CPT) and lapse rate tropopause temperature (LRT) within the ASMA in July and August 2015.
497 The July and August 2015 monthly mean tropopause parameters are removed from the respective
498 climatological monthly mean which is calculated by using COSMIC RO data from 2006 to 2014.

Formatted: Subscript

Formatted: Subscript

499 ~~One can note that we have strictly restricted our analysis within 40°N region for the cold point~~
500 ~~tropopause. Kindly noticed that the analysis is strictly restricted within the 45° N region for the~~
501 ~~cold point tropopause. Fig. Figure 10a-b (Fig. 10c-d) shows the CPT and LRT anomalies observed~~
502 in July (August) 2015. The tropopause temperature anomalies (CPT/LRT) also exhibit a distinct
503 pattern in July and August as observed in O₃ (Fig. 7). In July, the CPT/LRT anomalies show strong
504 positive anomalies (~5 K) in most of the ASMA region. High positive CPT/LRT anomalies are
505 also noticed over the ~~northwestern pacific~~ (NWP) region particularly below 20°N. These CPT/LRT
506 anomalies observed over the NWP region ~~are~~ might be due to the El Niño induced changes in the
507 Walker circulation and convective activity. Previous studies also observed significant warm
508 tropopause temperature anomalies over WP and maritime continent during the El Niño period
509 (~~Gettleman-Gettleman~~ et al., 2001). In August, the strong positive CPT/LRT anomalies (~5K) are
510 concentrated over the northeastern edges of the anticyclone where the ~~western pacific~~ WP mode of
511 the anticyclone ~~is was~~ separated from the ASMA. The temperature anomalies at 1 km above and
512 below the CPH also show similar behavior as seen in the CPT/LRT during August 2015 (~~figures~~
513 ~~not shown~~). Overall, the tropopause temperature anomalies in July and August 2015 within the
514 ASMA are well correlated with the strong enhancement in the O₃ as shown in Fig. 7. However,
515 the enhanced O₃ anomalies (heating due to the O₃) itself cannot explain the observed positive
516 tropopause temperature anomalies within the ASMA in 2015. This might be due to the El Niño
517 induced changes in the convective activity and the circulation. It is well known that the reversal of
518 walker circulation and the shifting of the convective activity (suppressed convective activity over
519 ASM region) are generally observed during the warm phase of ENSO. One can be noticed that
520 apart from the convection, other factors such as stratospheric QBO, atmospheric waves (gravity
521 waves and Kelvin waves) also strongly influenced the tropopause temperatures. It is concluded

Formatted: Superscript

Formatted: Font: Not Bold

Formatted: Subscript

Formatted: Subscript

that the enhanced O_3 within the ASMA is a main possible reason for the observed strong positive tropopause temperature anomalies in July and August 2015.

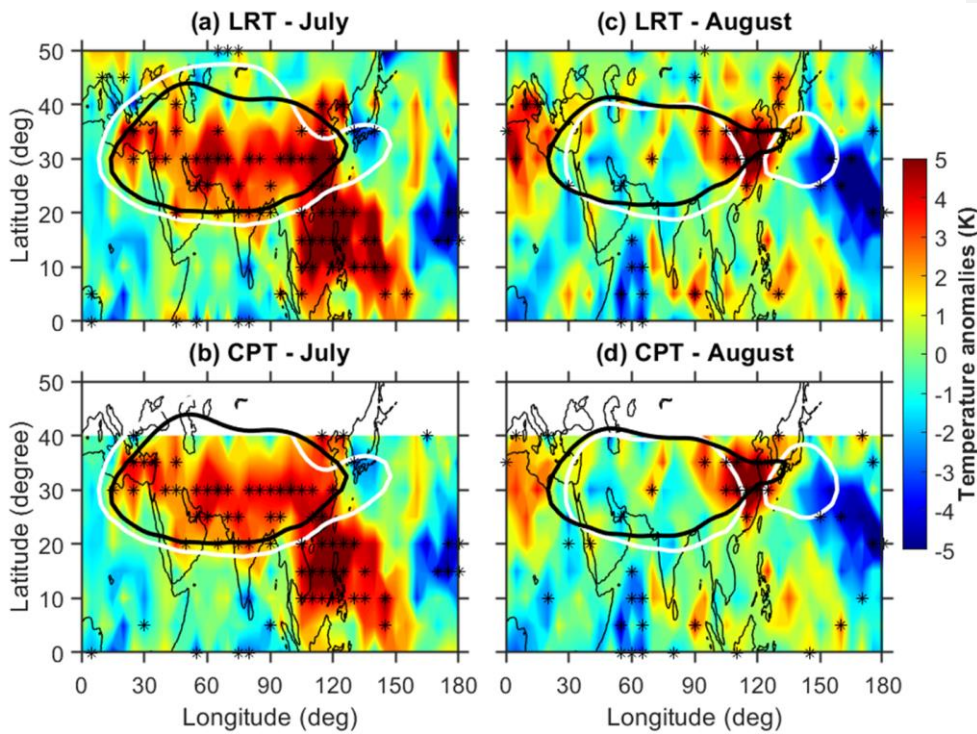


Figure 10. Spatial distribution of (a) lapse rate tropopause temperature (LRT), (b) cold point tropopause temperature (CPT) anomalies in July 2015. (c) and (d) same as (a) and (b) but for the month of August 2015. The white (black) color contour represents 16.75 km geopotential height at 100 hPa for the corresponding month in 2015 (mean of 2005-2014 climatological). The star symbols (black) shown in figure represent the anomalies greater than the $\pm 2\sigma$ standard deviation of long-term mean.

4. Summary and Conclusions

In this study, we investigated the detailed changes observed in the structure, dynamics and trace gases (Ozone, Water Vapor, Carbon Monoxide) variability within the ASMA in 2015 by using reanalysis products and satellite measurements observations. The tropopause temperature (CPT

535 and LRT) on monthly scales particularly during July and August 2015 also discussed. To quantify
536 the changes that happened within the ASMA region, 11 years (2005-2015) of O₃, WV and CO
537 observations from the Aura-MLS data and 10 years (2006-2015) of tropopause temperature data
538 from the COSMIC RO temperature profiles are used. The [NCEP-DOE Reanalysis 2](#) ~~NCEP~~
539 ~~reanalysis~~ observed winds and GPH data from 2005 to 2015 are also utilized. The results are
540 obtained by comparing the trace gas quantities in July and August 2015 with corresponding long-
541 term monthly mean quantities.

542 The trace gases within the ASMA exhibit substantial anomalous behavior in July and August
543 2015. During July and August 2015, we observed an enhancement of O₃ and the lowering of CO
544 and WV over most of the ASMA region. The decrease of the tropospheric tracers (CO and WV) is
545 quite expected due to the weaker upward motions from the weak monsoon ~~circulation~~ in 2015.
546 This is supported by a recent study reported by Fadnavis et al. (2019). They showed weaker upward
547 motions and deficient rainfall in the 2015 monsoon due to the strong El Niño conditions. However,
548 the strong enhancement in the stratospheric tracer (O₃) ~~over~~ within the ASMA particularly over
549 the northeastern edges of the ASMA during July is quite interesting. This is might be due to the
550 stratospheric intrusions as well as transport from the mid-latitudes. Based on Fishman and Seiler
551 (1983), it was stated that the positive correlation between CO and O₃ indicates, the O₃ is produced
552 by in-situ in the troposphere whereas the correlation is negative means the O₃ originates from the
553 stratosphere. We noticed a strong negative correlation between CO and O₃ in the present study
554 with increased O₃ and decreased CO from the MLS measurements. This clearly reveals that the
555 observed increased O₃ within the ASMA during 2015 is the stratospheric origin. This is further
556 supported by higher negative GPH anomalies associated with a southward meandering of the
557 subtropical westerly jet over northeastern Asia in July (**Fig. 3** and **4**). Further, the increased O₃ at

558 100 hPa and 121 hPa over western edges of the ASMA during August clearly indicates the transport
559 of the O₃ towards outer regions through the outflow of the ASMA (**Fig. 7e-f**). Interestingly, the
560 tropopause temperature obtained from the COSMIC RO data in July 2015 shows strong positive
561 temperature anomalies (~5 K) over the entire ASMA region. These warm tropopause temperatures
562 again supported the increased O₃ within the ASMA during 2015. The major findings obtained from
563 the present study are summarized in the following.

564 ❖ The spatial extension of the ASMA region shows higher than long-term mean except over
565 northeastern Asia where it exhibits a strong southward shift in July. Whereas in August, the
566 AMSA further separated into two anticyclones and the western Pacific mode anticyclone is
567 clearly evident in August.

568 ❖ The combination of Rossby wave breaking and pronounced southward meandering of
569 subtropical westerlies play a crucial role on the dynamical and structural changes in the
570 ASMA in 2015.

571 ❖ Strong enhancement in O₃ at 100 hPa (>40%) is clearly evident within the ASMA and
572 particularly higher over the northeastern edges of the ASMA in July. The enhanced O₃ is
573 strongly associated with a dominant southward meandering of the subtropical westerlies. In
574 August, the increased O₃ is significantly located over the western edges of the ASMA. This
575 clearly indicates the transport from the ASMA to the edges through its outflow.

576 ❖ A significant lowering of CO and WV within the ASMA is noticed during summer 2015. The
577 lowering of WV is higher at 146 hPa than 100 hPa. 30% (20%) decrease in CO (WV) is
578 observed within the ASMA in 2015. The decrease in the WV is higher at 146 hPa than 100
579 hPa.

580 ❖ Significant positive tropopause temperature anomalies (~5 K) is observed in the entire ASMA
581 region in July whereas, in August, the strong positive anomalies are concentrated over the
582 northeastern side of the ASMA.

583 The changes in the O₃ concentrations (increase/decrease) within the ASMA are one of the possible
584 mechanisms to strengthening/weakening of the ASMA (Braesicke et al., 2011). By using idealized
585 climate model experiments, Braesicke et al. (2011) clearly demonstrated that the strengthening
586 (weakening) of the ASMA occurred when the O₃ is decreased (increased) within the ASMA. The
587 increased O₃ within the ASMA warms the entire anticyclone region and weakens the ASMA
588 (Braesicke et al., 2011). Our results from the present study also in agreement with the results of
589 Braesicke et al. (2011). We also observed a pronounced increase of O₃ within the ASMA associated
590 with significant warming of tropopause as well as above and below the tropopause region in 2015.

591 By using precipitation index, wind data and stream functions, previous studies reported that the
592 ASMA circulation in 2015 was weaker than the normal (Tweedy et al., 2018; Yuan et al.,
593 20182019). Based on our present results, the strongly enhanced O₃ within the ASMA also might
594 be one of the plausible reasons for weakening of the ASMA in 2015. Based on our present results,
595 we conclude that the strong enhanced O₃ through the subtropical intrusions within the ASMA
596 region significantly warms around the tropopause region and caused an increase in the UTLS
597 temperature within the ASMA and indirectly leads to the weakening of the ASMA in 2015.

598 **Author contributions:** SRB designed the study, conducted research, performed initial data
599 analysis and wrote the first manuscript draft. MVR, GB, SKP and NHL edited the first manuscript.
600 All authors edited the paper.

601 **Data Availability:** All the data used in the present study is available freely from the respective
602 websites. The MLS trace gases data obtained from Earth Science Data website. The

603 ~~[NCEP Reanalysis 2 data provided by the NOAA/OAR/ESRL PSL, Boulder, Colorado, USA, from](http://www.cpc.ncep.noaa.gov/products/wesley/reanalysis2/kana/reanl2-1.htm)~~
604 ~~[their web site \(http://www.cpc.ncep.noaa.gov/products/wesley/reanalysis2/kana/reanl2-1.htm\)](http://www.cpc.ncep.noaa.gov/products/wesley/reanalysis2/kana/reanl2-1.htm)~~
605 ~~NCEP/NCAR reanalysis data are available from NOAA website~~
606 ~~<https://www.esrl.noaa.gov/psd/data/gridded/data.ncep.reanalysis.pressure.html>~~. The COSMIC
607 data is available from COSMIC CDAAC website (<http://cdaac->
608 www.cosmic.ucar.edu/cdaac/products.html).

609 **Competing interests:** The authors declare that they have no conflict of interest.

610 **Acknowledgments:** Aura MLS observations obtained from the GES DISC through their FTP site
611 (<https://mls.jpl.nasa.gov/index-eos-mls.php>) is highly acknowledged. We thank the COSMIC Data
612 Analysis and Archive Centre (CDAAC) for providing RO data used in the present study through
613 their FTP site (<http://cdaac-www.cosmic.ucar.edu/cdaac/products.html>). We also thank to
614 NCEP/NCAR reanalysis for providing geopotential and wind data. We thank ECMWF for
615 providing ERA interim reanalysis data.

616 **References**

- 617 Anthes, R., Bernhardt, P., Chen, Y., Cucurull, L., Dymond, K., Ector, D., Healy, S., Ho, S., Hunt,
618 D., Kuo, Y., Liu, H., Manning, K., McCormick, C., Meehan, T., Randel, W., Rocken, C.,
619 Schreiner, W., Sokolovskiy, S., Syndergaard, S., Thompson, D., Trenberth, K., Wee, T., Yen, N.,
620 and Zeng, Z.: The COSMIC/FORMOSAT-3 – Mission early results, *B. Am. Meteorol. Soc.*, 89,
621 313–333, 2008.
- 622 Avery, M. A., Davis, S. M., Rosenlof, K. H., Ye, H., Dessler, A. E., 2017. Large anomalies in lower
623 stratospheric water vapour and ice during the 2015–2016 El Niño, *Nat. Geosci.*, 10, 405–409,
624 <https://doi.org/10.1038/ngeo2961>.
- 625 ~~Barnston, A. G. and Livezey, R. E.: Classification, seasonality and persistence of low frequency~~
626 ~~atmospheric circulation patterns; *Mon. Weather Rev.* **115(6)** 1083–1126, 1987.~~
- 627 Basha, G., Ratnam, M. V., and Kishore, P.: Asian Summer Monsoon Anticyclone: Trends and
628 Variability, *Atmos. Chem. Phys. Discuss.*, <https://doi.org/10.5194/acp-2019-668>, in review,
629 2019.

630 Bergman, J. W., Fierli, F., Jensen, E. J., Honomichl, S., and Pan, L. L.: Boundary layer sources for
631 the Asian anticyclone: Regional contributions to a vertical conduit, *J. Geophys. Res.-Atmos.*,
632 118, 2560–2575, <https://doi.org/10.1002/jgrd.50142>, 2013.

633 Bian, J. C., Pan, L. L., Paulik, L., Vömel, H., and Chen, H. B.: In situ water vapor and ozone
634 measurements in Lhasa and Kunming during the Asian summer monsoon, *Geophys. Res. Lett.*,
635 39, L19808, <https://doi.org/10.1029/2012GL052996>, 2012.

636 Braesicke, P., O. J. Smith, P. Telford, and J. A. Pyle (2011), Ozone concentration changes in the
637 Asian summer monsoon anticyclone and lower stratospheric water vapour: An idealised model
638 study, *Geophys. Res. Lett.*, 38, L03810, doi:10.1029/2010GL046228.

639 Diallo, M., Riese, M., Birner, T., Konopka, P., Müller, R., Hegglin, M. I., Santee, M. L., Baldwin,
640 M., Legras, B., and Ploeger, F.: Response of stratospheric water vapor and ozone to the unusual
641 timing of El Niño and the QBO disruption in 2015–2016, *Atmos. Chem. Phys.*, 18, 13055–
642 13073, <https://doi.org/10.5194/acp-18-13055-2018>, 2018.

643 Das, S.S., Suneeth, K.V., Ratnam, M.V., Girach, I. A., Das, S. K.: Upper tropospheric ozone
644 transport from the sub-tropics to tropics over the Indian region during Asian summer monsoon,
645 *Clim Dyn.*, 52: 4567. <https://doi.org/10.1007/s00382-018-4418-6>, 2019.

646 Das, S., and Suneeth, K. V.: Seasonal and interannual variations of water vapor in the upper
647 troposphere and lower stratosphere over the Asian Summer Monsoon region- in perspective of
648 the tropopause and ocean-atmosphere interactions", *Journal of Atmospheric and Solar-*
649 *Terrestrial Physics* 201, 105244, doi:10.1016/j.jastp.2020.105244, 2020.

650 Dessler, A. E., Schoeberl, M. R., Wang, T., Davis, S. M., Rosenlof, K. H., and Vernier, J. P.:
651 Variations of stratospheric water vapor over the past three decades, *J. Geophys. Res. Atmos.*,
652 119, 12 588–12 598, doi:10.1002/2014JD021712, 2014.

653 Dunkerton, T. J.: The quasi-biennial oscillation of 2015–2016: Hiccup or death spiral?, *Geophys.*
654 *Res. Lett.*, 43, 10547–10552, <https://doi.org/10.1002/2016GL070921>, 2016.

655 Fadnavis, S. and Chattopadhyay, R.: Linkages of subtropical stratospheric intraseasonal intrusions
656 with Indian summer monsoon deficit rainfall, *J. Climate*, 30, 5083–5095,
657 <https://doi.org/10.1175/JCLI-D-16-0463.1>, 2017.

658 Fadnavis, S., Sabin, T.P., Roy, C. et al.: Elevated aerosol layer over South Asia worsens the Indian
659 droughts. *Sci Rep* 9, 10268, doi:10.1038/s41598-019-46704-9, 2019.

660 Fan, Q., Bian, J. and Pan, L. L.: Stratospheric entry point for upper-tropospheric air within the
661 Asian summer monsoon anticyclone, *Sci. China Earth Sci.*, 60, 1685–
662 1693, <https://doi.org/10.1007/s11430-016-9073-5>, 2017.

663 Fishman, J., and Seiler, W.: Correlative nature of ozone and carbon monoxide in the troposphere
664 - Implications for the tropospheric ozone budget; *J. Geophys. Res.* 88,
665 <https://doi.org/10.1029/JC088iC06p03662>, 1983.

666 Fueglistaler, S., Dessler, A. E., Dunkerton, T. J., Folkins, I., Fu, Q., and Mote, P. W.: Tropical
667 Tropopause Layer, *Rev. Geophys.*, 47, G1004+, <https://doi.org/10.1029/2008RG000267>, 2009.

668 Gadgil, S. and Francis, P. A.: El Niño and the Indian rainfall in June. *Curr Sci* 110:1010–1022,
669 2016.

670 Garny, H. and Randel, W. J.: Transport pathways from the Asian monsoon anticyclone to the
671 stratosphere, *Atmos. Chem. Phys.*, 16, 2703–2718, [https://doi.org/10.5194/acp-16-2703-](https://doi.org/10.5194/acp-16-2703-2016)
672 2016.

673 Gettelman, A., Randel, W. J., Massie, S., Wu, F.: El Niño as a natural experiment for studying the
674 tropical tropopause region, *J. Clim.*, 14, 3375– 3392, 2001.

675 Gettelman, A., Kinnison, D. E., Dunkerton, T. J., and Brasseur, G. P.: Impact of monsoon
676 circulations on the upper troposphere and lower stratosphere, *J. Geophys. Res.-Atmos.*, 109,
677 D22101, <https://doi.org/10.1029/2004JD004878>, 2004.

678 Highwood, E. J. and Hoskins, B. J.: The tropical tropopause, *Q. J. Roy. Meteor. Soc.*, 124, 1579–
679 1604, <https://doi.org/10.1002/qj.49712454911>, 1998.

680 Ho, S.-P., Anthes, R. A., Ao, C.O., Healy, S., Horanyi, A., Hunt, D., Mannucci, A.J., Pedatella, N.,
681 Randel, W.J., Simmons, A., Steiner, A., Xie, F., Yue, X., Zeng., Z.: The
682 COSMIC/FORMOSAT-3 radio occultation mission after 12 years: Accomplishments,
683 remaining challenges, and potential impacts of COSMIC-2. *Bull Amer Met Soc* 100 online
684 version: <https://journals.ametsoc.org/doi/pdf/10.1175/BAMS-D-18-0290.1>

685 Honomichl, S. B., and Pan, L. L.: Transport from the Asian summer monsoon anticyclone over the
686 western Pacific. *Journal of Geophysical Research: Atmospheres*, 125, e2019JD032094.
687 <https://doi.org/10.1029/2019JD032094>, 2020.

688 Hossaini, R., Chipperfield, M., Montzka, M. P., Rap, S. A., Dhomse, S., and Feng, W.: Efficiency
689 of short-lived halogens at influencing climate through depletion of stratospheric ozone, *Nat.*
690 *Geosci.*, 8, 186–190. <https://doi.org/10.1038/ngeo2363>, 2015.

691 ~~Jain, S., and Kar, S.C.: Transport of water vapour over the Tibetan Plateau as inferred from the~~
692 ~~model simulations. J. Atmos. Sol. Terr. Phys. 161, 64–75. [https://doi.org/](https://doi.org/10.1016/j.jastp.2017.06.016)~~
693 ~~[10.1016/j.jastp.2017.06.016](https://doi.org/10.1016/j.jastp.2017.06.016), 2017.~~

694 Jiang, J.H., Su, H., Zhai, C., Wu, L., Minschwaner, K., Molod, A.M., Tompkins, A.M.: An
695 assessment of upper troposphere and lower stratosphere water vapor in MERRA, MERRA2,
696 and ECMWF reanalyses using Aura MLS observations. *J. Geophys. Res. Atmos.* 120, 11.
697 <https://doi.org/10.1002/2015JD023752>, 468–11,485, 2015.

698 ~~Kanamitsu, M., Ebisuzaki, W., Woollen, J., Yang, S.-K., Hnilo, J. J., Fiorino, M., and Potter, G. L.:~~
699 ~~[NCEP-DOE AMIP-II Reanalysis \(R-2\), B. Am. Meteorol. Soc., 83, 1631–1643,](https://doi.org/10.1175/BAMS-83-11-1631)~~
700 ~~<https://doi.org/10.1175/BAMS-83-11-1631>, 2002.~~

701 ~~Kalnay, E., Kanamitsu, M., Kistler, R., Collins, W., Deaven, D., Gandin, L., Iredell, M., Saha, S.,~~
702 ~~White, G., Woollen, J., Zhu, Y., Leetmaa, A., Reynolds, R., Chelliah, M., Ebisuzaki, W.,~~
703 ~~Higgins, W., Janowiak, J., Mo, K. C., Ropelewski, C., Wang, J., Jenne, R., and Joseph, D.: The~~
704 ~~NCEP/NCAR 40 year reanalysis project, B. Am. Meteorol. Soc., 77, 437–471, 1996.~~

705 Khan, A., Jin, S.: Effect of gravity waves on the tropopause temperature, altitude and water vapor
706 in Tibet from COSMIC GPS Radio Occultation observations, *J. Atmos. Sol. Terr. Phys.* 138–
707 139, 23–31. <https://doi.org/10.1016/j.jastp.2015.12.001>, 2016.

708 Kim, J. and Son, S.-W.: Tropical Cold-Point Tropopause: Climatology, Seasonal Cycle, and
709 Intraseasonal Variability Derived from COSMIC GPS Radio Occultation Measurements, *J.*
710 *Climate*, 25, 5343–5360, <https://doi.org/10.1175/JCLI-D-11-00554.1>, 2012.

711 Kumar, K. K., Rajagopalan, B., Cane, M. A.: On the weakening relationship between the Indian
712 monsoon and ENSO. *Science* 287:2156–2159, 1999.

713 ~~Kunze, M., Braesicke, P., Langematz, U., Stiller, G., Bekki, S., Brühl, C., Chipperfield, M.,~~
714 ~~Dameris, M., Garcia, R., and Giorgetta, M.: Influences of the Indian Summer Monsoon on~~
715 ~~Water Vapor and Ozone Concentrations in the UTLS as Simulated by Chemistry Climate~~
716 ~~Models, J. Climate, 23, 3525–3544, <https://doi.org/10.1175/2010jcli3280.1>, 2010.~~

717 Kursinski, E. R., Hajj, G. A., Schofield, J. T., Linfield, R. P., and Hardy, K. R.: Observing Earth's
718 atmosphere with radio occultation measurements using the Global Positioning System, *J.*
719 *Geophys. Res.*, 102, 23429–23465, 1997.

720 ~~Konopka, P., Ploeger, F., Tao, M., and Riese, M.: Zonally resolved impact of ENSO on the~~
721 ~~stratospheric circulation and water vapor entry values, J. Geophys. Res.-Atmos., 121, 11486–~~

722 [11501, https://doi.org/10.1002/2015JD024698](https://doi.org/10.1002/2015JD024698), 2016.

723 Li, Q., Jiang, J. H., Wu, D. L., Read, W. G., Livesey, N. J., Waters, J. W., Zhang, Y., Wang, B.,
724 Filipiak, M. J., Davis, C. P., Turquety, S., Wu, S., Park, R. J., Yantosca, R. M., and Jacob, D.
725 J.: Convective outflow of South Asian pollution: A global CTM simulation compared with EOS
726 MLS observations, *Geophys. Res. Lett.*, 32, L14 826, <https://doi.org/10.1029/2005GL022762>,
727 2005.

~~728 Li J, Yu, R. and Zhou, T.: Teleconnection between NAO and climate downstream of the Tibetan
729 Plateau; *J. Climate* **21**(18), 4680–4690, 2008.~~

~~730 Li, D. and Bian, J.: Observation of a Summer Tropopause Fold by Ozone-sonde at Changchun,
731 China: Comparison with Reanalysis and Model Simulation, *Adv. Atmos. Sci.*, 32, 1354–1364,
732 <https://doi.org/10.1007/s00376-015-5022-x>, 2015.~~

733 Li, D., Vogel, B., Müller, R., Bian, J., Günther, G., Li, Q., Zhang, J., Bai, Z., Vömel, H., and Riese,
734 M.: High tropospheric ozone in Lhasa within the Asian summer monsoon anticyclone in 2013:
735 influence of convective transport and stratospheric intrusions, *Atmospheric Chemistry and
736 Physics*, 18, 17 979–17 994, <https://doi.org/10.5194/acp-18-17979-2018>, [https://www.atmos-
737 chem-phys.net/18/17979/2018/](https://www.atmos-chem-phys.net/18/17979/2018/), 2018.

~~738 Lin, Z.D. and Lu, R. Y.: Inter annual meridional displacement of the East Asian upper tropospheric
739 jet stream in summer. *Advances in Atmospheric Sciences*, 22, 199–211, 2005.~~

740 Livesey, N. J., Read, W. G., Wagner, P. A., Froidevaux, L., Lambert, A., Manney, G. L., Valle, L.
741 F. M., Pumphrey, H. C., Santee, M. L., Schwartz, M. J., Wang, S., Fuller, R. A., Jarnot, R. F.,
742 Knosp, B. W., and Martinez, E.: Version 4.2x Level 2 data quality and description document,
743 https://mls.jpl.nasa.gov/data/v4-2_data_quality_document.pdf, 2018

744 Nützel, M., Dameris, M., and Garny, H.: Movement, drivers and bimodality of the South Asian
745 High, *Atmos. Chem. Phys.*, 16, 14755–14774, <https://doi.org/10.5194/acp-16-14755-2016>,
746 2016.

747 Pan, L. L., Honomichl, S. B., Kinnison, D. E., Abalos, M., Randel, W. J., Bergman, J. W., and
748 Bian, J. C.: Transport of chemical tracers from the boundary layer to stratosphere associated
749 with the dynamics of the Asian summer monsoon, *J. Geophys. Res.-Atmos.*, 121, 14159–14174,
750 <https://doi.org/10.1002/2016JD025616>, 2016.

751 Park, M., Randel, W. J., Kinnison, D. E., Garcia, R. R., and Choi, W.: Seasonal variation of
752 methane, water vapor, and nitrogen oxides near the tropopause: Satellite observations and

753 model simulations, *J. Geophys. Res.-Atmos.*, 109, D03302,
754 <https://doi.org/10.1029/2003jd003706>, 2004.

755 Park, M., Randel, W. J., Gettelman, A., Massie, S. T., and Jiang, J. H.: Transport above the Asian
756 summer monsoon anticyclone inferred from Aura MLS tracers, *J. Geophys. Res.*, 112, D16309,
757 doi:10.1029/2006JD008294, 2007.

758 Park, M., Randel, W. J., Emmons, L. K., Bernath, P. F., Walker, K. A., and Boone, C. D.: Chemical
759 isolation in the Asian monsoon anticyclone observed in Atmospheric Chemistry Experiment
760 (ACE-FTS) data, *Atmos. Chem. Phys.*, 8, 757–764, <https://doi.org/10.5194/acp-8-757-2008>,
761 2008

762 Park, M., Randel, W. J., Emmons, L. K., and Livesey, N. J.: Transport pathways of carbon
763 monoxide in the Asian summer monsoon diagnosed from Model of Ozone and Related Tracers
764 (MOZART), *J. Geophys. Res.*, 114, D08303, <https://doi.org/10.1029/2008JD010621>, 2009.

765 Ramaswamy, C.: A preliminary study of the behavior of the Indian southwest monsoon in relation
766 to the westerly jet-stream. Special Palmen No. *Geophysica*, 6, pp. 455-476, 1958.

767 Randel, W. J. and Park, M.: Deep convective influence on the Asian summer monsoon anticyclone
768 and associated tracer variability observed with Atmospheric Infrared Sounder (AIRS), *J.*
769 *Geophys. Res.*, 111, D12314, <https://doi.org/10.1029/2005jd006490>, 2006.

770 ~~[Randel, W. J., Garcia, R. R., Calvo, N., and Marsh, D.: ENSO influence on zonal mean temperature
771 and ozone in the tropical lower stratosphere, *Geophys. Res. Lett.*, 36, L15822,
772 <https://doi.org/10.1029/2009GL039343>, 2009.](https://doi.org/10.1029/2009GL039343)~~

773 ~~[Randel, W. J., Park, M., Emmons, L., Kinnison, D., Bernath, P., Walker, K. A., Boone, C., and
774 Pumphrey, H.: Asian monsoon transport of trace gases to the stratosphere, *Science*, 328, 611–
775 613, 10.1126/science.1182274, 2010.](https://doi.org/10.1126/science.1182274)~~

776 Randel, W. J., Park, M., Emmons, L., Kinnison, D., Bernath, P., Walker, K. A., Boone, C., and
777 Pumphrey, H.: Asian Monsoon Transport of Pollution to the Stratosphere, *Science*, 328, 611–
778 613, <https://doi.org/10.1126/science.1182274>, 2010.

779 Rao, D.N., Ratnam, M.V., Mehta, S., Nath, D., Basha, G., Jagannadha Rao, V.V.M., et al:
780 Validation of the COSMIC radio occultation data over gadanki (13. 48°N, 79.2°E): A tropical
781 region, *Terr J Atmos Ocean Sci* 20, 59–70, [https://doi.org/10.3319/TAO.2008.01.23.01\(F3C\)](https://doi.org/10.3319/TAO.2008.01.23.01(F3C)),
782 2009.

783 RavindraBabu, S., VenkatRatnam, M., Basha, G., Krishnamurthy, B. V., and Venkateswararao, B.:
784 Effect of tropical cyclones on the tropical tropopause parameters observed using COSMIC GPS
785 RO data, *Atmos. Chem. Phys.*, 15, 10239–10249, doi:10.5194/acp-15-10239-2015, 2015.

786 RavindraBabu, S., VenkataRatnam, M., Basha, G., Liou, Y.-A., Narendra Reddy, N.: Large
787 Anomalies in the Tropical Upper Troposphere Lower Stratosphere (UTLS) Trace Gases
788 Observed during the Extreme 2015–16 El Niño Event by Using Satellite Measurements,
789 *Remote Sensing*, 2019, 11, 687. <https://doi.org/10.3390/rs11060687>, 2019. a

790 RavindraBabu, S., Venkat Ratnam, M., Basha, G., Krishnamurthy, B.V.: Indian summer monsoon
791 onset signatures on the tropical tropopause layer. *Atmos. Sci. Lett.* 20, e884.
792 <https://doi.org/10.1002/asl.884>, 2019. b

793 Ravindra Babu, S., Akhil Raj, S.T., Basha, G., Venkat Ratnam, M.: Recent trends in the UTLS
794 temperature and tropical tropopause parameters over tropical South Indian region, *J. Atmos.*
795 *Solar Terr. Phys.* 197:105164. <https://doi.org/10.1016/j.jastp.2019.105164>, 2020.

796 [Ravindra Babu, S. and Liou, Y. A.: Tropical tropopause layer evolution during 2015–16 El Niño
797 event inferred from COSMIC RO measurements, *J. Atmos. Solar Terr. Phys.* 212: 105507.
798 <https://doi.org/10.1016/j.jastp.2020.105507>](https://doi.org/10.1016/j.jastp.2020.105507)

799 Samanta, D., Dash, M. K., Goswami, B. N., and Pandey, P. C.: Extratropical anticyclonic Rossby
800 wave breaking and Indian summer monsoon failure. *Climate Dyn.*, 46, 1547–1562,
801 doi:<https://doi.org/10.1007/s00382-015-2661-7>, 2016.

802 Santee, M. L., Manney, G. L., Livesey, N. J., Schwartz, M. J., Neu, J. L., and Read, W. G.: A
803 comprehensive overview of the climatological composition of the Asian summer monsoon
804 anticyclone based on 10 years of Aura Microwave Limb Sounder measurements, *J. Geophys.*
805 *Res.-Atmos.*, 122, 5491–5514, <https://doi.org/10.1002/2016jd026408>, 2017.

806 Scherllin-Pirscher, B., Kirchengast, G., Steiner, A. K., Kuo, Y.-H., and Foelsche, U.: Quantifying
807 uncertainty in climatological fields from GPS radio occultation: an empirical-analytical error
808 model, *Atmos. Meas. Tech.*, 4, 2019–2034, doi:10.5194/amt-4-2019-2011, 2011a.

809 Scherllin-Pirscher, B., Steiner, A. K., Kirchengast, G., Kuo, Y.-H., and Foelsche, U.: Empirical
810 analysis and modeling of errors of atmospheric profiles from GPS radio occultation, *Atmos.*
811 *Meas. Tech.*, 4, 1875–1890, doi:10.5194/amt-4-1875-2011, 2011b.

812 [Shine, K. P. and Forster, P. M. D. F.: The effect of human activity on radiative forcing of climate
813 change: a review of recent developments, *Glob. Planet. Change*, 20, 205–225, 1999.](https://doi.org/10.1016/j.gloplacha.1999.02.001)

814 ~~Song, Y., Lü, D., Li, Q., Bian, J., Wu, X., and Li, D.: The impact of cut-off lows on ozone in the~~
815 ~~upper troposphere and lower stratosphere over Changchun from ozonesonde observations, *Adv.*~~
816 ~~*Atmos. Sci.*, 33, 135–150, <https://doi.org/10.1007/s00376-015-5054-2>, 2016.~~

817 Sprenger, M., Maspoli, M. C., and Wernli, H.: Tropopause folds and cross-tropopause exchange:
818 A global investigation based upon ECMWF analyses for the time period March 2000 to
819 February 2001, *J. Geophys. Res.*, 108, 8518, <https://doi.org/10.1029/2002JD002587>, 2003.

820 Škerlak, B., Sprenger, M., and Wernli, H.: A global climatology of stratosphere–troposphere
821 exchange using the ERA-Interim data set from 1979 to 2011, *Atmos. Chem. Phys.*, 14, 913–
822 937, <https://doi.org/10.5194/acp-14-913-2014>, 2014.

823 Tweedy, O. V., Waugh, D. W., Randel, W. J., Abalos, M., Oman, L. D., and Kinnison, D. E.: The
824 Impact of Boreal Summer ENSO Events on Tropical Lower Stratospheric Ozone, *Journal of*
825 *Geophysical Research: Atmospheres*, 123, 9843–9857, <https://doi.org/10.1029/2018JD029020>.

826 Uppala, S. M., Kållberg, P. W., Simmons, A. J., Andrae, U., da Costa Bechtold, V., Fiorino, M.,
827 Gibson, J. K., Haseler, J., Hernandez, A., Kelly, G. A., Li, X., Onogi, K., Saarinen, S., Sokka,
828 N., Allan, R. P., Andersson, E., Arpe, K., Balmaseda, M. A., Beljaars, A. C. M., van de Berg,
829 L., Bidlot, J., Bormann, N., Caires, S., Chevallier, F., Dethof, A., Dragosavac, M., Fisher, M.,
830 Fuentes, M., Hagemann, S., Hólm, E., Hoskins, B. J., Isaksen, I., Janssen, P. A. E. M., Jenne,
831 R., McNally, A. P., Mahfouf, J. F., Morcrette, J. J., Rayner, N. A., Saunders, R. W., Simon, P.,
832 Sterl, A., Trenberth, K. E., Untch, A., Vasiljevic, D., Viterbo, P., and Woollen, J.: The ERA-40
833 re-analysis, *Q. J. Roy. Meteor. Soc.*, 131, 2961–3012, <https://doi.org/10.1256/qj.04.176>, 2005.

834 Vellore, R. K., Kaplan, M. L., and Krishnan, R., et al.: Monsoon-extratropical circulation
835 interactions in Himalayan extreme rainfall; *Clim. Dyn.* **46**, 3517, 2016.
836 <https://doi.org/10.1007/s00382-015-2784-x>.

837 Venkat Ratnam, M., Ravindra Babu, S., Das, S. S., Basha, G., Krishnamurthy, B. V., and
838 Venkateswararao, B.: Effect of tropical cyclones on the stratosphere–troposphere exchange
839 observed using satellite observations over the north Indian Ocean, *Atmos. Chem. Phys.*, 16,
840 8581–8591, <https://doi.org/10.5194/acp-16-8581-2016>, 2016.

841 Vernier, J.-P., Thomason, L. W., and Kar, J.: CALIPSO detection of an Asian tropopause aerosol
842 layer, *Geophys. Res. Lett.*, 38, L07804, <https://doi.org/10.1029/2010GL046614>, 2011

843 Vernier, J.-P., Fairlie, T. D., Deshler, T., Ratnam, M. V., Gadhavi, H., Kumar, B. S., Natarajan,
844 M., Pandit, A. K., Raj, S. T. A., Kumar, A. H., Jayaraman, A., Singh, A. K., Rastogi, N., Sinha,

845 P. R., Kumar, S., Tiwari, S., Wegner, T., Baker, N., Vignelles, D., Stenchikov, G., Shevchenko,
846 I., Smith, J., Bedka, K., Kesarkar, A., Singh, V., Bhate, J., Ravikiran, V., Rao, M. D.,
847 Ravindrababu, S., Patel, A., Vernier, H., Wienhold, F. G., Liu, H., Knepp, T. N., Thomason,
848 L., Crawford, J., Ziemba, L., Moore, J., Crumeyrolle, S., Williamson, M., Berthet, G., Jégou,
849 F., and Renard, J.-B.: BATAL: The balloon measurement campaigns of the Asian tropopause
850 aerosol layer, *B. Am. Meteorol. Soc.*, 99, 955–973, [https://doi.org/10.1175/BAMS-D-17-](https://doi.org/10.1175/BAMS-D-17-0014.1)
851 0014.1, 2018.

852 Vogel, B., Günther, G., Müller, R., Groß, J.-U., Afchine, A., Bozem, H., Hoor, P., Krämer, M.,
853 Müller, S., Riese, M., Rolf, C., Spelten, N., Stiller, G. P., Ungermann, J., and Zahn, A.:
854 Longrange transport pathways of tropospheric source gases originating in Asia into the northern
855 lower stratosphere during the Asian monsoon season 2012, *Atmos. Chem. Phys.*, 16, 15301–
856 15325, <https://doi.org/10.5194/acp-16-15301-2016>, 2016.

857 Wang, B., Xiang, B., Li, J., Webster, P. J., Rajeevan, M. N., Liu, J., Ha, K. -J.: Rethinking Indian
858 monsoon rainfall prediction in the context of recent global warming. *Nat Commun* 6:7154.
859 doi:10.1038/ncomms8154, 2015.

860 Xu, X., Zhao, T., Lu, C., Guo, Y., Chen, B., Liu, R., Li, Y., Shi, X.: An important mechanism
861 sustaining the atmospheric “water tower” over the Tibetan Plateau. *Atmos. Chem. Phys.* 14,
862 11287–11295. <https://doi.org/10.5194/acp-14-11287-2014>.

863 Yan, R.-C., Bian, J.-C., and Fan, Q.-J.: The Impact of the South Asia High Bimodality on the
864 Chemical Composition of the Upper Troposphere and Lower Stratosphere, *Atmos. Ocean. Sci.*
865 *Lett.*, 4, 229–234, 2011.

866 Yan, R. C. and Bian, J. C.: Tracing the boundary layer sources of carbon monoxide in the Asian
867 summer monsoon anticyclone using WRF–Chem, *Adv. Atmos. Sci.*, 32, 943–951,
868 <https://doi.org/10.1007/s00376-014-4130-3>, 2015.

869 Yan, X., Konopka, P., Ploeger, F., Tao, M., Müller, R., Santee, M. L., Bian, J., and Riese, M.: El
870 Niño Southern Oscillation influence on the Asian summer monsoon anticyclone, *Atmospheric*
871 *Chemistry and Physics*, pp. 8079–8096, <https://doi.org/10.5194/acp-18-8079-2018>, 2018.

872 ~~Yang, S., Lau, K. M., Yoo, S. H., Kinter, J. L., Miyakoda, K. and Ho, C. H.: Upstream subtropical~~
873 ~~signals preceding the Asian summer monsoon circulation; *J. Climate*, 17, 4213–4229, 2004.~~

874 Yu, P., Rosenlof, K. H., Liu, S., Telg, H., Thornberry, T. D., Rollins, A. W., Portmann, R. W., Bai,
875 Z., Ray, E. A., Duan, Y., Pan, L. L., Toon, O. B., Bian, J., and Gao, R.-S.: Efficient transport of

876 tropospheric aerosol into the stratosphere via the Asian summer monsoon anticyclone,
877 Proceedings of the National Academy of Sciences, pp. 6972–6977,
878 <https://doi.org/10.1073/pnas.1701170114>, 2017.

879 Yuan, C., Lau, W. K. M., Li, Z., and Cribb, M.: Relationship between Asian monsoon strength and
880 transport of surface aerosols to the Asian Tropopause Aerosol Layer (ATAL): interannual
881 variability and decadal changes, *Atmos. Chem. Phys.*, 19, 1901-1913,
882 <https://doi.org/10.5194/acp-19-1901-2019>, 2019.

883 ~~Zhang, Q., Wu, G., and Qian, Y.: The Bimodality of the 100 hPa South Asia High and its~~
884 ~~Relationship to the Climate Anomaly over East Asia in Summer, *J. Meteorol. Soc. Jpn.*, 80,~~
885 ~~733–744, 2002.~~

886 ~~Zheng, B., Chevallier, F., Ciais, P., Yin, Y., Deeter, M. N., Worden, H. M., Wang, Y., Zhang, Q.,~~
887 ~~and He, K.: Rapid decline in carbon monoxide emissions and export from East Asia between~~
888 ~~years 2005 and 2016, *Environ. Res. Lett.*, 13, 044007, [https://doi.org/10.1088/1748-](https://doi.org/10.1088/1748-9326/aab2b3)~~
889 ~~9326/aab2b3~~, 2018.

890
891